

Red-Shifted Hydrogen Bonds and Blue-Shifted van der Waals Contact in the Standard Watson–Crick Adenine–Thymine Base Pair

Pan-Pan Zhou and Wen-Yuan Qiu*

State Key Laboratory of Applied Organic Chemistry, Department of Chemistry, Lanzhou University, 222 South Tianshui Road, Lanzhou, P. R. China

Received: April 17, 2009; Revised Manuscript Received: August 3, 2009

Standard Watson–Crick adenine–thymine (AT) base pair has been investigated by using the B3LYP functional with 6-31G(d, p) basis set, at which level of theory the geometrical characteristics of the AT base pair are the best in agreement with the experiment. It exhibits simultaneously red-shifted N–H···O and N–H···N hydrogen bonds as well as a blue-shifted C–H···O contact. AIM analysis suggests that the blue-shifted C–H···O contact exists as van der Waals interaction, and the electron density ρ that reflects the strength of a bond has been used to explain the red- and blue-shifted. By means of NBO analysis, we report a method to estimate the effect of hyperconjugation quantitatively, which combines the electron density in the X–H (X = N, C) σ bonding orbital with that in the σ^* antibonding orbital. The effect of structural reorganization on the origins of the red- and blue-shifted has been considered by the partial optimization, its behavior on the X–H (X = N, C) bond is quite different. Rehybridization and repolarization models are employed, and they act as bond-shortening effects. The competition between the electrostatic attractions and Pauli/nucleus repulsions is present in the two typical red-shifted N–H···O and N–H···N hydrogen bonds as well as in the blue-shifted C–H···O van der Waals contact. Electrostatic attraction between H and Y atoms (Y = O, N) is an important reason for the red shift, while the nucleus–nucleus repulsion between H and O atoms may be a factor leading to the C–H bond contraction and its blue shift. The electric field effect induced by the acceptor O atom on the C–H bond is also discussed.

1. Introduction

Hydrogen bonding and van der Waals interactions are two of the most important intermolecular interactions. Hydrogen bond X–H···Y is a force involving a covalent X–H bond of the proton donor (where X is an element with higher electronegativity than that of H, such as O, F, or N atom) and an electronegative proton acceptor Y (where Y is either an electronegative atom having one or more lone electron pairs, or a region of excess electron density such as aromatic π -electron system). It plays a key role in many chemical and biochemical processes.^{1–5} van der Waals interaction occurs between nonbonded atoms, molecules, and surfaces, which includes dipole–dipole, dipole–induced dipole, and London (dispersion) forces. It is still of considerable interest due to its great importance in chemistry, physics, and biology.^{6–8} These intermolecular interactions play crucial roles in the life system such as the structures of DNA and proteins.^{8–10} To explore their natures is extremely interesting and challenging.

It is well-known that the two helical chains of nucleotides in DNA are held together by the hydrogen bonds generated between a purine- and a pyrimidine-derived nucleic bases. In general, the base pairings are observed between adenine (A) and thymine (T) and between guanine (G) and cytosine (C), which lead to the so-called Watson–Crick AT and GC base pairs.^{9,10} Conventionally, it is believed that a Watson–Crick AT base pair is connected through the two typical N–H···O and N–H···N hydrogen bonds. In the past few decades, several studies^{11–13} have proposed the formation of a C–H···O hydrogen bond in the AT base pair. Recently, the theoretical

method of compliance constants is used to quantify the bond strengths^{14–16} and implies that a C–H···O contact may exist as a hydrogen bond with weak but non-negligible interaction strength in the AT base pair.^{17,18} However, the existence of the C–H···O hydrogen bond in the AT base pair has been questioned by some researchers. Shishkin et al.¹⁹ have ruled it out, because their computations at the HF/6-31G(d,p) level show that the C–H stretching vibrational frequency of adenine (A) in the base pair shifts to a higher value (blue shift), but the C–H bond length does not change. Guerra et al.²⁰ thought that the distance between the C–H bond and O atom is too large to be indicative of a hydrogen-bonding interaction (the distance between the atoms C and O is 3.63 Å, and it is 2.81 Å between H and O atoms at the BP86/TZ2P level). And more importantly, they did not find any donor–acceptor orbital interaction corresponding with a C–H···O hydrogen bond. On the other hand, some other studies show that there is a quite weak C–H···O interaction in the AT base pair contributing to its stability.^{21,22} It implies that the C–H···O contact in the AT base pair may exist but not as a hydrogen bond. It arouses our interest, and one aim of the present study is to explore the existing form of the C–H···O contact.

It has been observed that the AT base pair exhibits simultaneously red-shifted N–H···O and N–H···N hydrogen bonds and a small blue shift of the C–H stretching vibrational frequency in adenine (A) upon the base pair formation.¹⁹ It is known that the red shift is associated with the elongation of the X–H bond and a concomitant decrease of its stretching vibrational frequency, whereas the blue shift relates to the shortened X–H bond and its increased stretching vibrational frequency. These two types of hydrogen bonds have been the

* Corresponding author. E-mail: wyqiu@lzu.edu.cn. Tel: +86-931-8911356. Fax: +86-931-8912582.

subject of numerous theoretical studies that focus on their natures and origins, from a point of view either physical^{23–43} or chemical.^{44–49} The red-shifted hydrogen bonds are mainly ascribed to two facets. One is the electrostatic attraction between the higher electronegativity Y and the positive H, which elongates the X–H bond.^{3,4} The other one is the charge-transfer or hyperconjugative interactions between the proton donor and the proton acceptor.⁵⁰ The charge transfer from the proton acceptor Y to the σ^* antibonding orbital of the proton donor weakens and lengthens the X–H bond, thus leading to red-shifted stretching vibrational frequency of X–H bond. The explanations for the blue-shifted hydrogen bond are still under debate. The first one for the X–H bond contraction and the blue shift is due to the short-range repulsive forces faced by H atom in the complex when attempting stabilization.^{23–36} The second interpretation for the blue shift is believed to be the electric field effect induced by the electron donor Y, which causes the X–H bond to be shortened.^{23,24,37–43} Cubero et al.⁴⁴ have used the theory of atoms in molecules to determine the topological properties of the blue-shifted hydrogen bond interaction, and their results show that the blue shift is caused by the redistribution of electron density in the X–H bond induced upon complexation. Hobza and co-workers^{45–47} have explained the blue shift by a two-step mechanism: first, the dominant part of electron density of the proton acceptor Y is transferred to the remote part of the proton donor (i.e., mainly to the bonds linked to X–H bond or atoms linked to X) rather than to the σ^* antibonding orbital of the X–H bond; then a second effect of structural reorganization occurs in the proton donor system, leading to the X–H bond contraction with a concomitant blue shift of its stretching vibrational frequency. An important and well-established mechanism was put forward by Alabugin and co-workers.⁴⁸ They suggested that the balance of hyperconjugation and rehybridization/repolarization acts in opposite directions and governs the X–H bond length in the X–H \cdots Y hydrogen-bonded complex. When hyperconjugation dominates, the X–H bond is elongated and accompanied by a red shift of its stretching vibrational frequency. When the hyperconjugative interaction is weak and, the X-hybrid orbital in the X–H bond is able to undergo a sufficient change in polarization and hybridization, the dominant rehybridization/repolarization effect leads to a shortening of the X–H bond and a blue shift of its stretching vibrational frequency.⁴⁸ The rehybridization/repolarization theory is widely accepted in explaining the blue-shifted hydrogen bond. Recently, Inagaki et al.⁴⁹ emphasized that the enhancement of the localization of the σ bonding electrons in the proton donor can cause the blue shift. It enlightens us that we must also consider the importance of the electron density in the σ bonding orbital. Noticeably, the recent study by McDowell and Buckingham has shown that the charge-transfer mechanism proposed by Hobza and co-workers^{45–47} cannot be used to explain the blue shift in BF \cdots HCl and CO \cdots HCl complexes, since HCl is a diatomic molecule and it has only one bond into which the electron density can be transferred.⁵¹ Wang et al.²⁶ stated that the rehybridization theory⁴⁸ cannot interpret the blue shift in the hydrogen-bonded F–He–H \cdots Y (Y = N₂, CO, and He) complexes because the proton donor is incapable of rehybridization. But Alabugin et al.^{52,53} made a clear statement that the rehybridization model cannot be used for the analysis of hydrogen bond in the recently discovered new class of blue-shifted hypervalent complexes of HARF and HKrF molecules.^{35,36,54–57} It is because the bond rehybridization concept is not applicable to atoms that lack the valence p-shell vacancies required for effective hybrid formation, notably

closed-shell rare gas (Rg) atoms.⁵² They perfectly rationalized the blue shift in the hydrogen-bonded X–Rg–H \cdots Y complex. During the formation of the complex, repolarization of the Rg–H bond occurs through a mechanism based on rebalancing of resonance contributions involved in the 3c,4e X–Rg–H bond, and it leads to the Rg–H bond shortening and its blue shift.^{52,53} Although different viewpoints exist, they indeed provide important insights on the origin of the blue-shifted hydrogen bond. Some of these theories have been successfully used to interpret the red or blue shift occurring at the group not participating in a hydrogen bond.^{58–65} However, up to now, the studies about the red or blue shift occurring at the group involved in van der Waals interaction have rarely been reported. Hence, another aim of this work is to investigate the origins of the red-shifted N–H \cdots O and N–H \cdots N hydrogen bonds and the blue-shifted C–H \cdots O contact in AT base pair. We report a method and apply it to quantitatively estimating hyperconjugation effect on the origins of the red- and blue-shifted. Besides this, other effects of structural reorganization, rehybridization, and repolarization are critically examined. In the last section, we discuss the physical factors to achieve a comprehensive understanding on the origins of the red- and blue-shifted.

2. Theoretical Methods

All of the calculations were performed using the Gaussian 98 suite of programs.⁶⁶ Because the molecular structure and property strongly depend on the methods and basis sets, especially for the X–H bond length change upon the complexation,⁶⁷ it is necessary to select a better method and a basis set for the geometry optimization. Fortunately, the previous studies on the AT base pair provide convenience for us to make the B3LYP method with the 6-31G(d, p) basis set a better selection. As discussed in the Results and Discussion, the B3LYP method with the 6-31G(d, p) basis set performs better for the hydrogen-bonded AT base pair than other methods and basis sets. Therefore, in the present work, the structure and stretching vibrational frequency of the AT base pair were investigated at this level of theory both without (standard) and with counterpoise-corrected^{68,69} (CP) optimization. The effect of basis set superposition errors⁶⁹ (BSSE) on the geometries, stretching vibrational frequencies, and interaction energies were taken into account. The single A and T bases were also investigated at this level. The intermolecular interaction energy ΔE_{int} is calculated as $\Delta E_{\text{int}} = E_{\text{MN}}(\text{MN}) - E_{\text{M}}(\text{M}) - E_{\text{N}}(\text{N})$, where $E_{\text{MN}}(\text{MN})$, $E_{\text{M}}(\text{M})$, and $E_{\text{N}}(\text{N})$ stand for the total energy of the MN complex and the energies of the M and N monomers, respectively. The notations in parentheses are the corresponding basis sets used in the complex MN, and the monomers M and N, respectively. The CP interaction energy is calculated by $\Delta E_{\text{MN}}^{\text{CP}} = \Delta E_{\text{int}} + \delta_{\text{BSSE}}$, and δ_{BSSE} is the BSSE content of the interaction energy. Base-pairing enthalpy at 298.15 K and 1 atm ($\Delta H_{298.15}$) is calculated from $\Delta H_{298.15} = \Delta E_{\text{MN}}^{\text{CP}} - 298.15R$. Here, R is equal to 0.00198 kcal mol⁻¹ K⁻¹.

Atoms in molecules^{70,71} (AIM) analysis which can give evidence of the existence of hydrogen bond was performed at the B3LYP/6-31G(d,p) level using the AIMALL (Version 08.11.06) program.⁷² Natural bond orbital^{50,73–77} (NBO) analysis was carried out at the same level. It can provide information such as natural atomic charges, occupancies in NBOs, rehybridization, repolarization, hyperconjugation interaction, and the orbital energies of the donor orbital and the acceptor orbital. The hyperconjugative interaction energy can be expressed as $E^{(2)} = \Delta E_{ij} = -n^{\sigma} F_{ij}^2 / (E_j - E_i)$, where n^{σ} is the donor orbital occupancy, $F_{(i,j)}$ is the off-diagonal NBO Fock matrix element,

and E_i and E_j are the donor and acceptor orbital energies, respectively.

The electron density–bond length relationship used to check the bond length change is elaborated here. It is known that the electron density changes for a certain single bond in a molecule directly affect the property of the molecular system. It involves the electron density in its bonding orbital and antibonding orbital, which play important roles in the bonding process. The bonding orbital is the region between two nuclei where electron density builds up. Electrons in such an orbital tend to draw atoms together to form a bond, and they are in favor of the stability of the molecule. The antibonding orbital is formed with the formation of each bonding orbital, which tends to localize electrons outside the region between two nuclei. Electrons in an antibonding orbital work against the formation of a bond and destabilize the molecule. The electron densities in the bonding orbital and antibonding orbital are closely correlated with the bond order and the bond length. In terms of the molecular orbital (MO) theory, the bond order S for a certain single bond in a molecule can be represented as⁷⁸

$$S = \frac{n^\sigma - n^{\sigma^*}}{2} \quad (1)$$

where n^σ and n^{σ^*} are the amount of electrons occupied in the σ bonding orbital and σ^* antibonding orbital, respectively.

In another way, the bond order S can be calculated from the observed bond length r using the Brown–Altermatt formula^{79,80}

$$S = \exp\left(\frac{r_0 - r}{B}\right) \quad (2)$$

where r_0 is the average bond length of a certain single bond determined by experiment and B is the empirical universal constant which equals to 0.37 Å.

Accordingly, the following equation can be deduced from Equations 1 and 2,

$$r = r_0 - 0.37 \ln \frac{n^\sigma - n^{\sigma^*}}{2} \quad (3)$$

It indicates that the bond length r is determined by not only the electron density in the σ^* antibonding orbital but also the one in the σ bonding orbital.

Therefore, upon the complex formation such as in the $X-H\cdots Y$ hydrogen-bonded system or van der Waals interaction, the $X-H$ bond length variation Δr can be calculated by

$$\Delta r = 0.37 \ln \frac{n_{\text{monomer}}^\sigma - n_{\text{monomer}}^{\sigma^*}}{n_{\text{complex}}^\sigma - n_{\text{complex}}^{\sigma^*}} \quad (4)$$

3. Results and Discussion

3.1. Dependence of the Optimized Geometry of the AT Base Pair on the Level of Theory. The available data in the literature^{20,22,81–88} for the $X\cdots Y$ distances of the AT base pair studied by Hartree–Fock (HF), B3LYP, BP86, and post-SCF [MP2, RI-MP2] theories with different basis sets are listed in Table 1 for comparison.

The $X\cdots Y$ distance of the AT base pair determined by experiment^{89,90} can be seen from Table 1. We used them as the

TABLE 1: Comparisons of the $X\cdots Y$ Distance (Å) in the AT Base Pair at Different Levels of Theory with Experiments

level of theory	$r(N6\cdots O4)$	$r(N1\cdots N3)$
HF/3-21G(d) ^a	2.973	2.779
HF/6-31G(d) ^a	3.071	2.994
HF/6-31G(d,p) ^a	3.081	2.990
B3LYP/3-21G(d) ^a	2.856	2.690
B3LYP/6-31G(d) ^a	2.948	2.876
B3LYP/6-31G(d,p) ^a	2.940	2.848
B3LYP/6-31++G(d,p) ^a	2.939	2.875
HF/6-31G(d,p) ^b	3.090	2.990
HF/cc-pVTZ(-f) ^c	3.060	2.920
BP86/TZ2P ^{d,e}	2.850	2.810
B3LYP/6-31G(d,p) ^f	2.940	2.845
MP2/6-31G(d) ^g	2.990	2.880
MP2/6-31G(d,p) ^g	2.970	2.840
RI-MP2/cc-pVTZ ^h	2.860	2.830
MP2/6-31+G(d,p) ⁱ	2.957	2.854
X-ray ^j	2.940	2.835

^a Reference 81. ^b Reference 82. ^c Reference 83. ^d Reference 20. ^e References 84 and 85. ^f Reference 86. ^g Reference 87. ^h Reference 88. ⁱ Reference 22. ^j References 89 and 90.

benchmarks for the selection of a proper method and a basis set. It is known that the discrepancy between theory and experiment regarding hydrogen bond lengths in Watson–Crick base pairs is mainly resulted from the molecular environment (water, sugar hydroxyl groups, counterions).^{20,84,85} In contrast with the data of the $X\cdots Y$ distances in the AT base pair calculated by HF, BP86, and post-SCF [MP2, RI-MP2] methods with different basis sets, and even with larger basis set, the results obtained at the B3LYP/6-31G(d, p) level^{81,86} have the smaller discrepancies relative to the experimental results.^{89,90} Therefore, under the conditions of not considering the effects of the molecular environment, the calculated $X\cdots Y$ distances in the AT base pair which are closer to the experimental values can reveal the interactions between A and T bases more exactly. This establishes that the B3LYP method with 6-31G(d, p) basis set can offer accurate and reliable results. The previous studies on other hydrogen-bonded systems have demonstrated that the B3LYP functional indeed can predict reliable results,^{91–97} and in particular, it is quite efficient in terms of computational time.^{98,99} Therefore, the B3LYP method may be a very appropriate selection for investigating the AT base pair of such big hydrogen-bonded complex. It can be seen from Table 1 that the moderate 6-31G(d, p) basis set is quite effective in giving satisfactory calculated geometries of the AT base pair. But generally speaking, the larger the basis set is, the better the description of the studied system will be. It makes us think about the basis set effects. Hence, we make a comparison of the optimized geometries of the AT base pair calculated with different basis sets using the B3LYP method, followed by vibrational frequency calculations to confirm the actual minima obtained. The results are illustrated in Table 2.

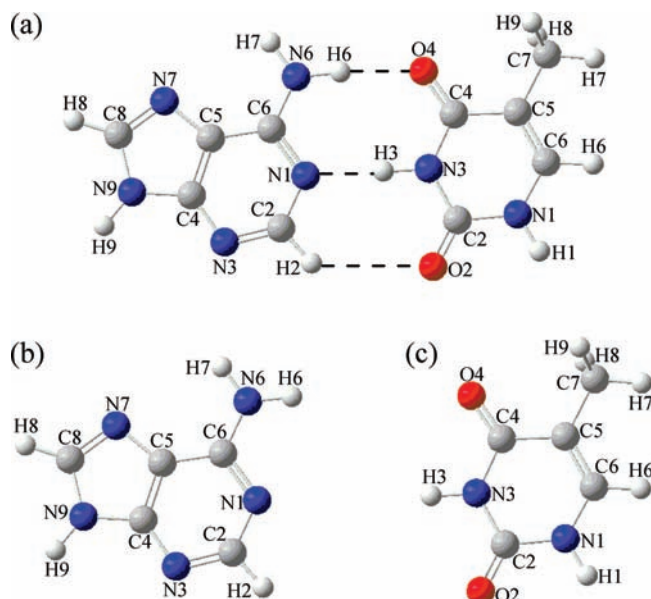
As presented in Table 2, the results show that the optimized geometry of the AT base pair at the B3LYP/6-31G(d, p) level are consistent with the previous studies,^{81,86} and they are closer to the experimental data^{89,90} than those with other basis sets that have more basis functions. The basis set affects the geometry to a different extent. Moreover, despite the state-of-the-art Dunning correlation consistent basis set¹⁰⁰ aug-cc-pVDZ are used, we find the optimized geometry of the AT base pair to be less than satisfactory. It indicates that in some cases a moderate basis set would have an advantage leading to satisfactory structure over the large basis set with more basis functions.¹⁰¹

TABLE 2: X···Y Distance (Å) in the AT Base Pair Calculated by Using the B3LYP Method with Different Basis Sets

level of theory	$r(N6\cdots O4)$	$r(N1\cdots N3)$
B3LYP/6-31G(d,p)	2.93934	2.84502
B3LYP/6-31G(d,2p)	2.93533	2.84435
B3LYP/6-31G(d,3p)	2.92920	2.84736
B3LYP/6-31G(d,pd)	2.93183	2.83576
B3LYP/6-31G(d,2pd)	2.93024	2.83761
B3LYP/6-31G(d,3pd)	2.92281	2.83705
B3LYP/6-31G(2d,p)	2.93473	2.83806
B3LYP/6-31G(2d,2p)	2.93380	2.83826
B3LYP/6-31G(2d,3p)	2.92706	2.83794
B3LYP/6-31G(2d,pd)	2.91913	2.82115
B3LYP/6-31G(2d,2pd)	2.92126	2.82420
B3LYP/6-31G(2d,3pd)	2.91566	2.82352
B3LYP/6-31G(3d,p)	2.92540	2.85269
B3LYP/6-31G(3d,2p)	2.92340	2.84819
B3LYP/6-31G(3d,3p)	2.92768	2.85320
B3LYP/6-31G(3d,pd)	2.91925	2.84288
B3LYP/6-31G(3d,2pd)	2.92101	2.84429
B3LYP/6-31G(3d,3pd)	2.92346	2.84499
B3LYP/6-31G(df,p)	2.94023	2.84935
B3LYP/6-31G(df,2p)	2.93623	2.84833
B3LYP/6-31G(df,3p)	2.93179	2.85199
B3LYP/6-31G(df,pd)	2.93512	2.84126
B3LYP/6-31G(df,2pd)	2.93206	2.84165
B3LYP/6-31G(df,3pd)	2.92781	2.84392
B3LYP/6-31G(2df,p)	2.93383	2.84123
B3LYP/6-31G(2df,2p)	2.93183	2.84224
B3LYP/6-31G(2df,3p)	2.93005	2.84530
B3LYP/6-31G(2df,pd)	2.92400	2.83138
B3LYP/6-31G(2df,2pd)	2.92318	2.83259
B3LYP/6-31G(2df,3pd)	2.91916	2.83317
B3LYP/6-31G(3df,p)	2.92750	2.85769
B3LYP/6-31G(3df,2p)	2.92507	2.85338
B3LYP/6-31G(3df,3p)	2.93011	2.85914
B3LYP/6-31G(3df,pd)	2.92422	2.85055
B3LYP/6-31G(3df,2pd)	2.92480	2.84925
B3LYP/6-31G(3df,3pd)	2.92645	2.85283
B3LYP/6-31+G(d,p)	2.94276	2.87360
B3LYP/6-31++G(d,p)	2.94273	2.87345
B3LYP/6-311G(d,p)	2.94407	2.86812
B3LYP/6-311+G(d,p)	2.94208	2.88673
B3LYP/6-311++G(d,p)	2.94224	2.88676
B3LYP/aug-cc-pVDZ	2.91745	2.86612

Furthermore, the X···Y distances in the AT base pair obtained by using the B3LYP method with the 6-31G(d,p) basis set (see Table 2) are compared with those calculated by MP2 method^{22,87} (see Table 1). It can be observed that the N6···O4 and N3···N1 distances at the MP2/6-31G(d) and MP2/6-31+G(d,p) levels of theory are relatively overestimated, while at the MP2/6-31G(d,p) level of theory, the N6···O4 distance is overestimated, and the N3···N1 distance is close to the value at the B3LYP/6-31G(d,p) level of theory. Thus, the B3LYP/6-31G(d,p) level of theory was selected for all subsequent calculations in this work because of its relatively small computational cost, particularly for its reliable and convincing geometrical structures about the AT base pair.

3.2. Geometries, Stretching Vibrational Frequencies, Interaction Energies and Base-Pairing Enthalpy. Optimized structures of the AT base pair and A and T bases are presented in Figure 1. Geometrical characteristics, stretching vibrational frequencies, and interaction energies of the AT base pair determined by standard and counterpoise-corrected (CP) optimizations at the B3LYP/6-31G(d, p) level are listed in Table 3, together with the base-pairing enthalpy. The corresponding parameters of the single bases A and T are summarized in Table 4.

**Figure 1.** Optimized structures of (a) Watson–Crick adenine–thymine (AT) base pair, (b) adenine (A), and (c) thymine (T) bases.**TABLE 3: Geometric Characteristics (d and R , in Å), Stretching Vibrational Frequencies (cm^{-1}), Interaction Energies ΔE_{int} (kcal mol^{-1}), and Base-Pairing Enthalpy $\Delta H_{298.15}$ (kcal mol^{-1}) of the AT Base Pair with Standard and CP Optimizations at the B3LYP/6-31G(d,p) Level**

	standard	CP
$d(H6\cdots O4)$	1.92061	1.93203
$d(N6\cdots O4)$	2.93934	2.95004
$R(N6-H6)^a$	1.02187 (0.01448)	1.02059 (0.01320)
$\nu(N6-H6)^b$	3407.2 (-208.3)	3422.9 (-192.6)
$d(N1\cdots H3)$	1.79619	1.85593
$d(N1\cdots N3)$	2.84502	2.90006
$R(N3-H3)^a$	1.04883 (0.03602)	1.04422 (0.03141)
$\nu(N3-H3)^b$	2953.9 (-665.6)	3037.2 (-582.3)
$d(H2\cdots O2)$	2.80003	2.92098
$d(C2\cdots O2)$	3.62967	3.73416
$R(C2-H2)^a$	1.08769 (-0.00027)	1.08787 (-0.00009)
$\nu(C2-H2)^b$	3191.4 (12.9)	3187.5 (9.0)
ΔE_{int}^c	-16.40	-12.45 (3.95)
$\Delta H_{298.15}^d$		-13.04

^a Values in parentheses are bond length variations of the AT base pair relative to those of the single bases (Table 4). ^b Values in parentheses are vibrational frequency shifts of the AT base pair relative to those of the single bases (Table 4). ^c Value in parentheses is the BSSE content of the interaction energy (δ_{BSSE}). ^d $\Delta H_{298.15}$ is the bond enthalpy at 298.15 K.

TABLE 4: Geometric Characteristics and Stretching Vibrational Frequencies of A and T Bases at the B3LYP/6-31G(d,p) Level^a

	bond	R	ν
A	N6–H6	1.00739	3615.5
	C2–H2	1.08796	3178.5
T	N3–H3	1.01281	3619.5

^a Bond lengths (R) are in Å. Stretching vibrational frequencies (ν) are in cm^{-1} .

From Table 3, it can be seen that the distance between H6 atom of the A base and O4 atom of the T base is smaller than the sum of their van der Waals radii (2.6 Å), and the distance between the N1 atom of the A base and the H3 atom of the T base is less than the sum of their van der Waals radii (2.7 Å), regardless of standard or counterpoise correction optimization.

The following van der Waals radii are taken into account: H (1.2 Å), O (1.4 Å), and N (1.5 Å).¹⁰² These results indicate the existence of N6–H6···O4 and N3–H3···N1 hydrogen bonds according to the geometrical criterion of the hydrogen bond.¹⁰³ But the distance between the H2 atom of the A base and the O2 atom of the T base is larger than the sum of their van der Waals radii (2.6 Å). Can the C2–H2···O2 contact exist as a hydrogen bond? As the case stands, we cannot exclude the C2–H2···O2 contact in the AT base pair as a hydrogen bond, because the H···Y distance is not shorter than the sum of their van der Waals radii in all hydrogen bonds.¹⁰⁴ Another existing form of the contact might be van der Waals interaction. The geometrical criteria¹⁰³ are direct but not convincing; therefore, we will further clarify their existing forms in the subsequent section.

The calculated N6···O4 and N1···N3 distances in the AT base pair using the standard optimization are consistent with the previous theoretical^{81,86} and experimental studies.^{89,90} While under the condition of counterpoise correction optimization, their values are overestimated (see Table 3). Whatever standard or counterpoise correction optimization is considered, both N6–H6 and N3–H3 bond lengths in the AT base pair are elongated relative to those in A and T bases (see Tables 3 and 4). The N3–H3 bond length is elongated more than that of the N6–H6 bond, and there is a larger decrease of the N3–H3 stretching vibrational frequency than that of the N6–H6 bond. It means that both N6–H6···O4 and N3–H3···N1 hydrogen bonds are red-shifted. The stretching vibrational frequency of the C2–H2 bond shifts to a higher value that coincides with the earlier result.¹⁹ But, strikingly, its bond length contracts, whereas the C2–H2 bond length remains unchanged in the earlier result.¹⁹ The reason may be that the larger X···Y distances in the AT base pair at the HF/6-31G(d,p) level^{81,82} seriously deviate from the experimental values^{89,90} and the factual interactions between A and T bases cannot be simulated (see Table 1). Contrarily, the results at the B3LYP/6-31G(d,p) level would reveal the actual situations in the AT base pair. Therefore, the AT structure optimized without counterpoise correction (standard) will be adopted in the following analyses. The interaction energy of the AT base pair without counterpoise correction (–16.40 kcal mol⁻¹) is in good agreement with the previous studies.^{81,105} After counterpoise correction, the interaction energy (–12.45 kcal mol⁻¹) is approximate to the studies by Guerra et al.^{20,85} and Bertran et al.⁸⁶ The computed B3LYP/6-31G(d,p) base-pairing enthalpy for the Watson–Crick AT base pair is –13.04 kcal mol⁻¹, which agrees well with the experimental results of –12.10 kcal mol⁻¹,¹⁰⁶ deviating by as little as –0.94 kcal mol⁻¹ (see Table 3). It confirms that the moderate B3LYP/6-31G(d,p) level is capable of providing reliable interaction energy for the AT base pair. In this respect, it is believed that the CCSD(T) interaction energy is highly accurate,^{107–112} but with a much greater computation time. It shows that the computations at the moderate B3LYP/6-31G(d,p) level are feasible for such a large complex as the AT base pair, which is out of reach for the current technology of CCSD(T). CP optimization influences the geometries, stretching vibrational frequencies, and interaction energy to a different extent. Compared to the standard calculations, the N6–H6, N3–H3, and C2–H2 bond lengths obtained by CP-corrected calculations are obviously shorter, their stretching vibrational frequencies are smaller, and the interaction energy is larger.

3.3. Electron Density Topological Analysis. The electron density topological analyses of the AT base pair and A and T bases were performed at the B3LYP/6-31G(d,p) level. Accord-

TABLE 5: Topological Parameters of the Bond Critical Points and Ring Critical Points in the AT Base Pair, and of the X–H (X = N, C) Bonds in the AT Base Pair, A and T Bases at the B3LYP/6-31G(d,p) Level^a

		ρ	$\nabla^2\rho$	λ_1	λ_2	λ_3
BCP						
AT	H6···O4	0.02745	0.07532	–0.03655	–0.03580	0.14767
	N1···H3	0.04355	0.09561	–0.06891	–0.06547	0.22999
	H2···O2	0.00499	0.01806	–0.00463	–0.00426	0.02696
	N6–H6	0.32824	–1.77079	–1.34063	–1.28469	0.85453
	N3–H3	0.30655	–1.62273	–1.25718	–1.21809	0.85254
	C2–H2	0.29448	–1.13652	–0.83462	–0.80083	0.49894
A	N6–H6	0.34344	–1.83089	–1.33738	–1.26893	0.77541
	C2–H2	0.29256	–1.10684	–0.82055	–0.78552	0.49922
T	N3–H3	0.34151	–1.84209	–1.34389	–1.28900	0.79079
RCP						
AT	C6 N6 H6 O4	0.00494	0.02231	–0.00398	0.00955	0.01674
	C4 N3 H3 N1					
	N1 C2 H2 O2	0.00339	0.01492	–0.00249	0.00494	0.01248
	C2 N3 H3					

^a All the units are in au.

ing to the AIM theory proposed by Bader,^{70,71} the electron density ρ is used to describe the strength of a bond. The larger ρ value means the stronger bond. The Laplacian value $\nabla^2\rho$ of the electron density ρ is used to characterize the bond. It is expressed as $\nabla^2\rho = \lambda_1 + \lambda_2 + \lambda_3$, where λ_i is an eigenvalue of the Hessian matrix of ρ . When one of the three eigenvalues is positive and the other two are negative, we denote it by (3, –1) and call it the bond critical point (BCP). When one is negative and the other two are positive, it is denoted as (3, +1) and is named as the ring critical point (RCP), which indicates the existence of a ring structure. As Bader^{70,71} pointed out, there are two classes of the atomic interactions: the negative $\nabla^2\rho$ means the interatomic bond exists as the covalent bond, while the positive $\nabla^2\rho$ suggests that the bond belongs to the ionic bond, hydrogen bond, or van der Waals interaction. Popelier^{113,114} proposed eight criteria for the existence of hydrogen bond, and Lipkowski et al.¹¹⁵ pointed out that three are the most fundamental and are often applied; that is, there exists a bond critical point, and the electron density (ρ) and its Laplacian ($\nabla^2\rho$) should be within the ranges 0.002–0.035 and 0.024–0.139 au, respectively.

The topological parameters of the bond critical points and ring critical points are outlined in Table 5. The ρ values for H6···O4, N1···H3, and H2···O2 in the AT base pair are 0.02745, 0.04355, and 0.00499 au, respectively. They do fall within the proposed ranges above. The $\nabla^2\rho$ values for H6···O4 and N1···H3 are in the range from 0.024 to 0.139 au, it proves the existences of N6–H6···O4 and N1···H3–N3 hydrogen bonds. The small ρ (H2···O2) value (0.00499 au) is consistent with the values of the previous studies about van der Waals complexes, approximately 10⁻³ au in van der Waals complexes.^{70,116–119} In addition, the $\nabla^2\rho$ value for H2···O2 is 0.01806 au, which is out of the region of 0.024–0.139 au, and it is smaller than 0.024 au; thus these two phenomena indicate that the H2···O2 interaction exists as a van der Waals interaction. The topological analysis shows that there are three intramolecular rings (the subsystem A base possesses a five-membered ring and a six-membered ring, and the subsystem T base has a intramolecular six-membered ring) and two intermolecular rings in the AT base pair. Here we do not show the topological parameters of the three intramolecular rings but only the two intermolecular rings (see Table 5). The first intermolecular ring critical point listed in Table 5 shows that the H6···O4 and N1···H3 interactions must exist so as to form the eight-membered ring. Similarly, there must be the N1···H3 and

TABLE 6: NBO Occupancies in the the X–H (X = N, C) σ Bonding Orbital and σ^* Antibonding Orbital of the AT Base Pair and A and T Bases at the B3LYP/6-31G(d,p) Level and the Calculated r Value of the X–H (X = N, C) Bond Length and the Relative Bond Length Variation Δr

	bond	n^σ ^a	n^{σ^*} ^a	r ^b	Δr
AT	N6–H6	1.98827 (–0.00100)	0.04302 (0.03314)	1.02027 (0.16%)	0.00644
	N3–H3	1.97590 (–0.00622)	0.08290 (0.06813)	1.03034 (1.76%)	0.01425
	C2–H2	1.97863 (–0.00083)	0.02571 (–0.00033)	1.09881 (1.02%)	0.00009
A	N6–H6	1.98927	0.00988	1.01383 (0.64%)	
	C2–H2	1.97946	0.02604	1.09872 (0.99%)	
T	N3–H3	1.98212	0.01477	1.01609 (0.32%)	

^a Values in parentheses are NBO occupancies variations of the AT base pair relative to those of the single bases. The units are in electrons.

^b Values in parentheses are the relative errors between r and R . The units are in Å.

H2...O2 interactions that lead to the formation of the seven-membered ring. Therefore, it reconfirms the existence of the C–H...O interaction in the AT base pair. By comparison of the electron density ρ of the X–H (X = N, C) bond in the AT base pair with those of A and T single bases, we can know the bond strength and bond length variation. The greater the localization of the electron density at the bond critical point is, the greater the bond strength is and, the shorter the bond length is.¹²⁰ On the other hand, it is generally believed that the greater the strength of the bond is, the higher the stretching vibrational frequency is, and vice versa.¹²¹ As shown in Table 5, the values $\rho(\text{N6–H6})$ and $\rho(\text{N3–H3})$ in the AT base pair are smaller than those of A and T single bases. It suggests that the N6–H6 and N3–H3 bond in the AT base pair become weaker after the hydrogen bond formation; thus it is elongated, and its stretching vibrational frequency shifts to a lower value. But the $\rho(\text{C2–H2})$ in the AT base pair increases by a few compared to that in the A single base; thus the C2–H2 bond becomes stronger and it is shortened and its stretching vibrational frequency shifts to a higher value. From this point of view, the red-shifted N6–H6 and N3–H3 bonds can be attributed to the decrease of electron density upon AT base pair formation, while the increase of electron density in the C2–H2 bond results in its blue shift.

3.4. NBO Analysis. To get more information on the origins of the red-shifted N6–H6 and N3–H3 bonds and blue-shifted C2–H2 bond, NBO analysis has been carried out at the B3LYP/6-31G(d,p) level.

First of all, the hyperconjugation effect is considered. The importance of hyperconjugation has been well-documented⁵⁰ and has been extensively used to explain the red- and blue-shifted hydrogen bonds.^{45–48,122–138} The red-shifted hydrogen bond is caused by $n(\text{Y})$ or $\pi(\text{Y}) \rightarrow \sigma^*(\text{X–H})$ hyperconjugative interaction, because such interaction leads to an increase of electron density in the X–H σ^* antibonding orbital. As a result, the X–H bond is weakened and elongated accompanied by a red shift of its stretching vibrational frequency.⁵⁰ The blue-shifted hydrogen bond results from the competition between the intramolecular hyperconjugative interaction $n(\text{Z})$ or $\sigma(\text{Z–W}) \rightarrow \sigma^*(\text{X–H})$ and the intermolecular hyperconjugative interaction $n(\text{Y}) \rightarrow \sigma(\text{Y–U}) \rightarrow \sigma^*(\text{X–H})$ (in the Z(or Z–W)–X–H...Y(or Y–U) hydrogen-bonded system). The larger decrements of the energy of the intramolecular hyperconjugative interaction $n(\text{Z}) \rightarrow \sigma(\text{Z–W}) \rightarrow \sigma^*(\text{X–H})$ make the electron density in the X–H σ^* antibonding orbital decrease and finally strengthens the X–H bond, leading to its contraction and a blue shift of its stretching vibrational frequency.^{134–136} These studies qualitatively elucidate the hyperconjugation effect on the origins of the red- and blue-shifted hydrogen bonds. But how can we explain them quantitatively? It is solved now on the basis of the electron density–bond length relationship.

According to eqs 3 and 4, it can be known that the electron density in the X–H σ bonding orbital is also very important,

TABLE 7: NBO Analysis of A and T Bases and the AT Base Pair at the B3LYP/6-31G(d,p) Level^a

	A	T	AT
$E^{(2)}_{[\text{LP}(1)\text{O4} \rightarrow \text{BD}^*(1)\text{N6–H6}]}$ (kcal mol ^{–1})			5.94
$E^{(2)}_{[\text{LP}(2)\text{O4} \rightarrow \text{BD}^*(1)\text{N6–H6}]}$ (kcal mol ^{–1})			9.87
$E^{(2)}_{[\text{LP}(1)\text{N1} \rightarrow \text{BD}^*(1)\text{N3–H3}]}$ (kcal mol ^{–1})			30.74
$E^{(2)}_{[\text{LP}(1)\text{O2} \rightarrow \text{BD}^*(1)\text{C2–H2}]}$ (kcal mol ^{–1})			0.18
$E^{(2)}_{[\text{LP}(2)\text{O2} \rightarrow \text{BD}^*(1)\text{C2–H2}]}$ (kcal mol ^{–1})			0.43
$q^{\text{H6}}(\text{N6–H6})$ (electrons)	0.42690		0.44948
$q^{\text{H3}}(\text{N3–H3})$ (electrons)		0.45478	0.47309
$q^{\text{H2}}(\text{C2–H2})$ (electrons)	0.21910		0.23687
$sp^n(\text{N6–H6})$	$sp^{2.41}$		$sp^{2.05}$
% s-character	29.28		32.76
$sp^n(\text{N3–H3})$		$sp^{2.65}$	$sp^{2.27}$
% s-character		27.39	30.60
$sp^n(\text{C2–H2})$	$sp^{2.18}$		$sp^{2.11}$
% s-character	31.42		32.13
$\text{pol}(\sigma_{\text{N6–H6}})\text{N6}\%$	71.66		74.12
$\text{pol}(\sigma^*_{\text{N6–H6}})\text{N6}\%$	28.34		25.88
$\text{pol}(\sigma_{\text{N3–H3}})\text{N3}\%$		73.20	76.79
$\text{pol}(\sigma^*_{\text{N3–H3}})\text{N3}\%$		26.80	23.21
$\text{pol}(\sigma_{\text{C2–H2}})\text{C2}\%$	61.40		62.33
$\text{pol}(\sigma^*_{\text{C2–H2}})\text{C2}\%$	38.60		37.67

^a BD denotes σ bonding orbital; BD* denotes σ^* antibonding orbital; LP denotes valence lone pair. For BD and BD*, (1) denotes σ orbital, (2) denotes π orbital. For LP, (1) and (2) denote the first and the second lone pair electron, respectively.

and its crucial role has been qualitatively emphasized by Wang and Hobza.¹³⁹ The previous studies rarely took the electron density in the X–H σ bonding orbital into account on the origins of the red- and blue-shifted, due to its considerably small variation upon the hydrogen bond formation. In this work, the electron density in the X–H σ bonding orbital as well as that in its σ^* antibonding orbital will be considered together to quantitatively estimate their effects on the origins of the red- and blue-shifted.

NBO occupancies in the X–H (X = N, C) σ bonding orbital and σ^* antibonding orbital of the AT base pair, A and T single bases are presented in Table 6. It can be seen that all the n^σ in the X–H (X = N, C) bonds of the AT base pair slightly decrease when compared with those of A and T bases. Both the n^{σ^*} in N6–H6 and N3–H3 bonds of the AT base pair increase, but the n^{σ^*} in the C2–H2 bond of the AT base pair decreases. NBO analysis shows that the σ bonding orbital and σ^* antibonding orbital of the X–H (X = N, C) bond in the AT base pair both participate in the intermolecular and intramolecular hyperconjugations. The increase of the N6–H6 σ^* antibonding orbital occupancies n^{σ^*} is mainly caused by the two pairs of intermolecular donor–acceptor orbital interactions: $\text{LP}(1)\text{O4} \rightarrow \text{BD}^*(1)\text{N6–H6}$ and $\text{LP}(2)\text{O4} \rightarrow \text{BD}^*(1)\text{N6–H6}$, whose energies are 5.94 and 9.87 kcal mol^{–1}, respectively (see Table 7). And these two pairs of orbital interactions are plotted in Figure 2a,b,

respectively, using Molekel 4.3.¹⁴⁰ The LP(1)O4→BD*(1)N6–H6 orbital interactions overlap sideways, while the LP(2)O4→BD*(1)N6–H6 orbital interactions overlap head-to-head, which are stronger. There are some other donor orbitals interact with the N6–H6 σ^* antibonding orbital (BD*(1)N6–H6), but their interaction energies are very small (see Table S1 in Supporting Information). In terms of the rough estimation 0.001 electrons of charge transfer corresponds to 1 kcal mol⁻¹ of the stabilization energy,¹²⁴ their contributions to the increase of N6–H6 σ^* antibonding orbital occupancies are minor. By comparing the intramolecular donor–acceptor orbital interaction energies related to the N6–H6 σ^* antibonding orbital in the AT base pair with those in A base, we can obtain the contributions of the intramolecular hyperconjugations (see Tables S1 and S2 in Supporting Information). The results suggest that the intramolecular hyperconjugations only result in a slight decrease of N6–H6 σ^* antibonding orbital occupancies. With respect to the N6–H6 σ bonding orbital occupancies, both the intermolecular and intramolecular hyperconjugations act as decreasing effects. The increase of the N3–H3 σ^* antibonding orbital occupancies arises primarily from the donating adenine orbital with N1 lone-pair character: LP(1)N1→BD*(1)N3–H3, the interaction energy is 30.74 kcal mol⁻¹. Their orbitals have a large overlap, which indicates a strong interaction (see Figure 2c). And its increase resulting from the other intermolecular donor orbitals is small; the intramolecular hyperconjugations increase the N3–H3 σ^* antibonding orbital occupancies to a minor extent. Because the intermolecular hyperconjugations related to the N3–H3 σ bonding orbital are weak, they only slightly decrease the N3–H3 σ bonding orbital occupancies. The intramolecular hyperconjugations notably decrease the N3–H3 σ bonding orbital occupancies (see Tables S1 and S2 in Supporting Information). To our surprise, contrary to the previous study,²⁰ there are two very weak intermolecular donor–acceptor orbital interactions corresponding to the C2–H2...O2 contact: LP(1)O2→BD*(1)C2–H2 and LP(2)O2→BD*(1)C2–H2 (see Table 7, and Figure 2d,e), these two pairs of orbitals are very close to each other but their orbitals have no overlapping. They increase the C2–H2 σ^* antibonding orbital occupancies slightly. But the intramolecular hyperconjugations act as decreasing effects. There are no intermolecular hyperconjugations relevant to the C2–H2 σ bonding orbital, and the intramolecular hyperconjugations increase the C2–H2 σ bonding orbital occupancies but to a small extent (see Tables S1 and S2 in Supporting Information).

From the above analysis, it can be seen that the intermolecular and intramolecular hyperconjugations work together and lead to electron density redistribution within the proton donor. They adjust the electron density in the X–H (X = N, C) bond upon AT base pair formation. They cannot be detached from each other because they are cooperative. Thus, the resulting changes of the n^σ and n^{σ^*} in the X–H (X = N, C) bond can be attributed to a couple of the two interactions.

For the sake of calculating the r and Δr values according to eqs 3 and 4, we select the standard single N–H and C–H bond lengths as $r_{0,\text{NH}} = 1.01 \text{ \AA}$, $r_{0,\text{CH}} = 1.09 \text{ \AA}$. Table 6 lists the calculated values. Compared to the R value at the B3LYP/6-31G(d,p) level with standard optimization, the bond lengths r calculated by eq 3 are very approximate, and the relative errors between them are about 1%. It confirms the validation of eq 3. The Δr values for N6–H6 and N3–H3 bonds in the AT base pair suggest that they are elongated, and it is consistent with the aforementioned results. The reasons originate from both the decrease of the σ bonding orbital occupancies and the increase

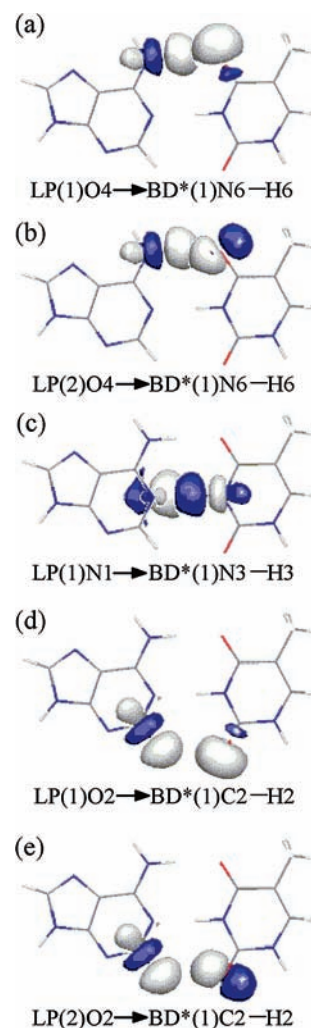


Figure 2. Intermolecular hyperconjugation interactions between natural bond orbitals in the AT base pair.

of the σ^* antibonding orbital occupancies. The data in Table 6 show that the C2–H2 σ^* antibonding orbital occupancies decrease by 0.00033 electrons. It may be a reason for the shortened C2–H2 bond and its blue shift based on the above theory.^{134–136} However, it is observed that the C2–H2 bond in the AT base pair has a relatively small elongation according to eq 3. It should be noted that the C2–H2 σ bonding orbital occupancies also decrease (by 0.00083 electrons), which elongate the C2–H2 bond. Due to the larger decrements of the C2–H2 σ bonding orbital occupancies, its bond lengthens finally. As a consequence, the C–H blue shift cannot be ascribed to the decrease of electron density in its σ^* antibonding orbital. It is contrary to the above theories.^{134–136} Hence, it can be concluded that the hyperconjugation is a bond lengthening effect for the X–H (X = N, C) bond in the AT base pair. The result is different from our previous study in which the hyperconjugation acts as a bond shortening effect.¹⁴¹ Furthermore, it indicates that, to estimate the hyperconjugation effect, the electron density in the X–H σ^* antibonding orbital as well as that of its σ bonding orbital must be taken into account together.

3.5. Effect of Structural Reorganization. Hobza et al.⁴⁵ emphasized that the second effect of structural reorganization is an important reason for the blue-shifted hydrogen bond. But the theoretical study of the blue-shifted hydrogen bond in the HCHO...HNO complex suggests that structural reorganization cannot be the fundamental reason for the blue shift because it can only lead to a small contraction of the N–H bond length

TABLE 8: Changes of the X–H (X = N, C) Bond Lengths and Stretching Vibrational Frequencies in the Partial Optimized A and T Bases Relative to Those of All Optimized A and T Bases at the B3LYP/6-31G(d,p) Level

subsystem	bond	R'^a	ν'^b
A	N6–H6	1.00669 (–0.00070)	3619.6 (4.1)
	C2–H2	1.08820 (0.00024)	3176.2 (–2.3)
T	N3–H3	1.01307 (0.00382)	3615.6 (–3.9)

^a Values in parentheses are bond length variations relative to the monomers (Table 4). The units are in Å. ^b Values in parentheses are vibrational frequency shifts relative to the monomers (Table 4). The units are in cm^{-1} .

and a slight blue shift of its stretching vibrational frequency.¹²⁵ The same conclusion is also derived from the study of the $\text{N–H}\cdots\text{H–B}$ blue-shifted dihydrogen bond in the $\text{BH}_3\text{NH}_3\cdots\text{HNO}$ complex.¹⁴² But after comparison, we find that the X–H bond contraction resulting from structural reorganization by their partial optimizations are of the same order of magnitude as the contraction upon the complex formation. It shows that structural reorganization may indeed play a key role in the blue shift. To deepen the understanding of structural reorganization effect on the (X = N, C) bond in the AT base pair, the effects of changes of other bond lengths on the X–H bond length were studied. In this process, the subsystems A and T are taken from the optimized AT base pair, and the bond lengths of the subsystem remain unchanged with the exception of the X–H (X = N, C) bond whose bond length is set equal to that in the single A or T base. The partial optimizations on them are then performed at B3LYP/6-31G(d,p) level. It should be emphasized that the effects of changes of bond angles or dihedral angles are not discussed here since these values cannot be kept frozen during the optimization. The corresponding results are summarized in Table 8. After the base pair formation, the bond length changes affect the X–H (X = N, C) bond to a different extent. It can be seen from Tables 3 and 4 that the N6–H6 and N3–H3 bonds in the AT base pair are red-shifted, up to 208.3 and 665.6 cm^{-1} , respectively, while the C2–H2 bond is blue-shifted about 12.9 cm^{-1} . Surprisingly, due to structural reorganization, a blue shift of 4.1 cm^{-1} is observed for the N6–H6 bond, and the bond is shortened by 0.00070 Å, but the C2–H2 and N3–H3 bonds are red-shifted by 2.3 and 3.9 cm^{-1} , respectively, and both of them are elongated. These results point out that structural reorganization has a different effect on the X–H (X = N, C) bond. In regard to the red-shifted N6–H6 \cdots O4 hydrogen bond, structural reorganization acts as a bond shortening effect and results in the blue shift, while for the red-shifted N3–H3 \cdots N1 hydrogen bond and blue-shifted C2–H2 \cdots O2 van der Waals contact, it acts as bond lengthening effect and leads to the red shift. Therefore, the behavior of structural reorganization on the X–H bond in the noncovalent interaction (such as hydrogen-bonding interaction or van der Waals interaction) may be quite different.

3.6. Effects of Rehybridization and Repolarization. Recently, Alabugin et al.⁴⁸ proposed that repolarization and rehybridization are the main factors for the blue-shifted hydrogen bond. They observed that upon the X–H \cdots Y hydrogen bond formation, the X–H bond polarization increases, echoed by the increase of the positive charge on the hydrogen atom, which leads to an increase of the s-character in the X hybrid orbital according to Bent's rule.¹⁴³ Both effects result in the X–H bond shortening and its blue shift. As can be seen from Table 7, the results obtained are consistent with the repolarization and rehybridization model. In the AT base pair, the polarizations

TABLE 9: Magnitudes of the Five Factors on the X–H (X = N, C) Bond Length in the AT Base Pair at the B3LYP/6-31G(d,p) Level

bond	$\Delta r/\Delta r^a$	Rh/ Δr^b	Rp/ Δr^c	$\Delta R'/\Delta r^d$
N6–H6	44.48%	– (shortening)	– (shortening)	–4.83%
N3–H3	39.56%	– (shortening)	– (shortening)	10.61%
C2–H2	–33.33%	+ (shortening)	+ (shortening)	–88.89%

^a The hyperconjugation (intermolecular and intramolecular) effect, Δr , is taken from Table 6, and Δr is the difference of the X–H (X = N, C) bond lengths between the AT base pair in Table 3 (without CP) and the single A or T base in Table 4. ^b Rh represents rehybridization effect. ^c Rp represents repolarization effect. ^d The structural reorganization effect, $\Delta R'$, is the difference of the X–H (X = N, C) bond length between the subsystems in Table 8 and the single A or T base in Table 4.

of N6–H6, C2–H2, and N3–H3 σ bonding orbitals all increase relative to those in A and T bases, whereas the polarizations of their σ^* antibonding orbitals decrease. They cooperate together and give rise to an increase of the polarization of X–H (X = N, C) bond, which acts as bond shortening effect. The s-characters of the N6, C2, and N3 hybrid orbitals in N6–H6, C2–H2, and N3–H3 bonds also increase as presented in the sp^n hybridization. The n values decrease upon the base pair formation; it implies that the orbital overlapping between X (X = N, C) and H atomic orbitals becomes stronger and more effective, and it makes the X–H (X = N, C) bond become stronger and contracted. Summarily, both repolarization and rehybridization behave as bond shortening effects. The facts that the N6–H6 and N3–H3 bonds in the AT base pair are elongated suggest that the shortening effects of repolarization and rehybridization cannot dominate. In contrast, the two effects may play important roles in the C2–H2 bond contraction. These conclusions have been confirmed by the subsequent discussion.

4. Evaluations of the Proportions of the Five Factors

From the above analyses, it can be seen that there are five factors (intermolecular and intramolecular hyperconjugations, structural reorganization, rehybridization, and repolarization) associated with the origins of the red-shifted N6–H6 \cdots O4 and N3–H3 \cdots N1 hydrogen bonds and the blue-shifted C2–H2 \cdots O2 van der Waals contact in the AT base pair. Herein, we obtain the proportions of the X–H (X = N, C) bond length variations caused by these factors to the factual X–H (X = N, C) bond length variations upon the base pair formation, as shown in Table 9. The X–H (X = N, C) bond length caused by the hyperconjugation (intermolecular and intramolecular) effect can be quantitatively estimated by combining the electron density in the X–H (X = N, C) σ bonding orbital with that of its σ^* antibonding orbital. Structural reorganization effects on the X–H (X = N, C) bond length can also be known quantitatively. Compared to the N6–H6 bond elongation upon the base pair formation, the elongation caused by hyperconjugation takes up less than 45%, while the structural reorganization acts as a negative effect. With regard to the N3–H3 bond, the hyperconjugation effect accounts for about 40%, and it is about 10% for structural reorganization. Whereas for the C2–H2 bond, both hyperconjugation and structural reorganization act as negative effects. Rehybridization and repolarization lead to bond contractions for the X–H (X = N, C) bond in the AT base pair, but quantitative estimates of their effects on the X–H (X = N, C) bond length have not been realized. In total, the five factors take up less than 40% on the origin of the red-shifted N6–H6 \cdots O4 hydrogen bond, and smaller than 50% on the

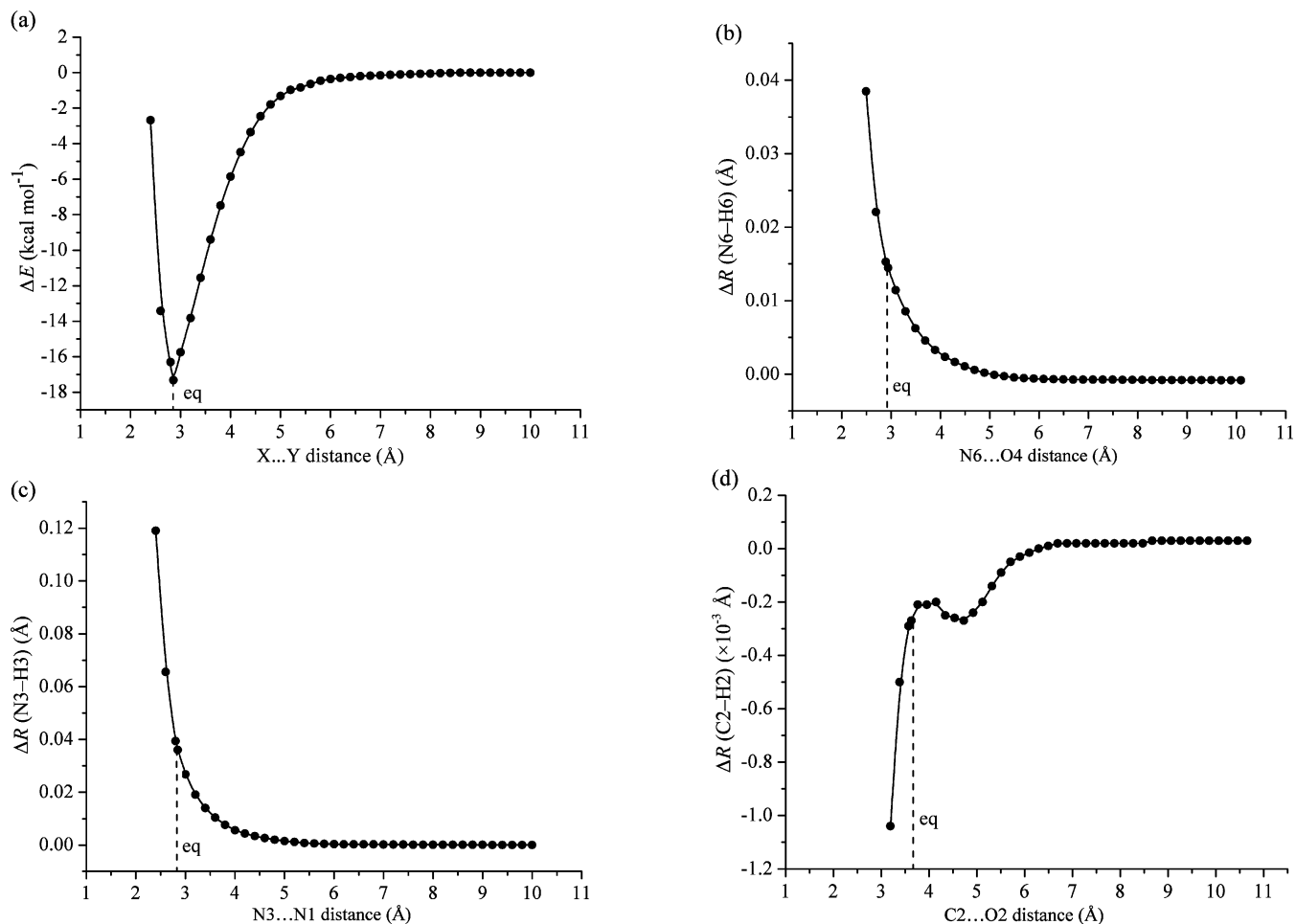


Figure 3. Interaction energy and the optimized X–H (X = N, C) bond length as a function of the X...Y distance between the proton donor and acceptor: (a) X = N3 (N6 or C2) and Y = N1 (O4 or O2); (b) N6–H6 bond; (c) N3–H3 bond; (d) C2–H2 bond. (Equilibrium X...Y distances are denoted by the lines labeled “eq”.)

origin of the red-shifted N3–H3...N1 hydrogen bond, the remaining percentages should be explained by the physical factors. But with respect to the blue-shifted C2–H2...O2 van der Waals contact, the negative effects of hyperconjugation and structural reorganization are considerably large; therefore, rehybridization and repolarization must play important roles in the C2–H2 bond contraction, and the physical factors should be considered as well.

5. Physical Origins

To understand the physical origins of the red-shifted N6–H6...O4 and N3–H3...N1 hydrogen bonds, and blue-shifted C2–H2...O2 van der Waals contact in the AT base pair, the N3...N1 distance is changed step by step. By fixing the N3...N1, N6...O4, and C2...O2 distances at each step and then optimizing the remaining coordinates of the complex, we obtain curves of the interaction energy and the optimized X–H (X = N, C) bond length as a function of the X...Y distance (see Figure 3). NBO analysis and AIM analysis are performed at each step to examine the interactions during the process of the base pair formation.

The potential energy curve represents the energy variation in the process of the base pair formation, as shown in Figure 3a. At the large distance, the interaction between A and T bases are electrostatic attraction, the interaction energy gradually becomes negative to a small extent as the X...Y (X = N or C, Y = O) distance decreases. The bond critical points (BCP) of

N1...H3 and O4...H6 start to appear at 6.7 and 5.5 Å of the N1...N3 distance, respectively. But the electron density ρ and the positive Laplacian $\nabla^2\rho$ for N1...H3 at 6.7 Å, and these values for N1...H3 and O4...H6 at 5.5 Å are very small and not within the proposed ranges being as hydrogen bond.¹¹⁵ It suggests that the interactions between A and T bases belong to van der Waals interactions at these distances. NBO analysis shows that there a very weak intermolecular hyperconjugative interaction (LP(1)N1→RY*(1)H3, $E^{(2)} = 0.06$ kcal mol⁻¹) appears along the N1→H3–N3 direction at 5.0 Å of the N1...N3 distance. It still exists as van der Waals interaction confirming by AIM analysis, in which the $\rho(\text{N1}\cdots\text{H3})$ is 0.00027 au, its Laplacian $\nabla^2\rho(\text{N1}\cdots\text{H3})$ is 0.00127 au, and the $\rho(\text{O4}\cdots\text{H6})$ and $\nabla^2\rho(\text{O4}\cdots\text{H6})$ are 0.00011 and 0.00071 au, respectively. Intermolecular hyperconjugative interactions gradually appear along this direction and become stronger as the decreasing N1...N3 distance. At 4.6 Å of the N1...N3 distance, another very weak intermolecular hyperconjugative interaction (LP(2)O4→RY*(1)H6, $E^{(2)} = 0.06$ kcal mol⁻¹) along the O4→H6–N6 direction occurs. AIM analysis indicates that the interactions between A and T bases are van der Waals interactions at this point ($\rho(\text{N1}\cdots\text{H3}) = 0.00082$ au, $\nabla^2\rho(\text{N1}\cdots\text{H3}) = 0.00322$ au, and $\rho(\text{O4}\cdots\text{H6}) = 0.00036$ au, $\nabla^2\rho(\text{O4}\cdots\text{H6}) = 0.00189$ au). The appearance of the bond critical points (BCP) of O2...H2 at 4.0 Å of the N1...N3 distance is indicative of the forming C2–H2...O2 van der Waals contact. It can be seen from Figure 3a that there is a

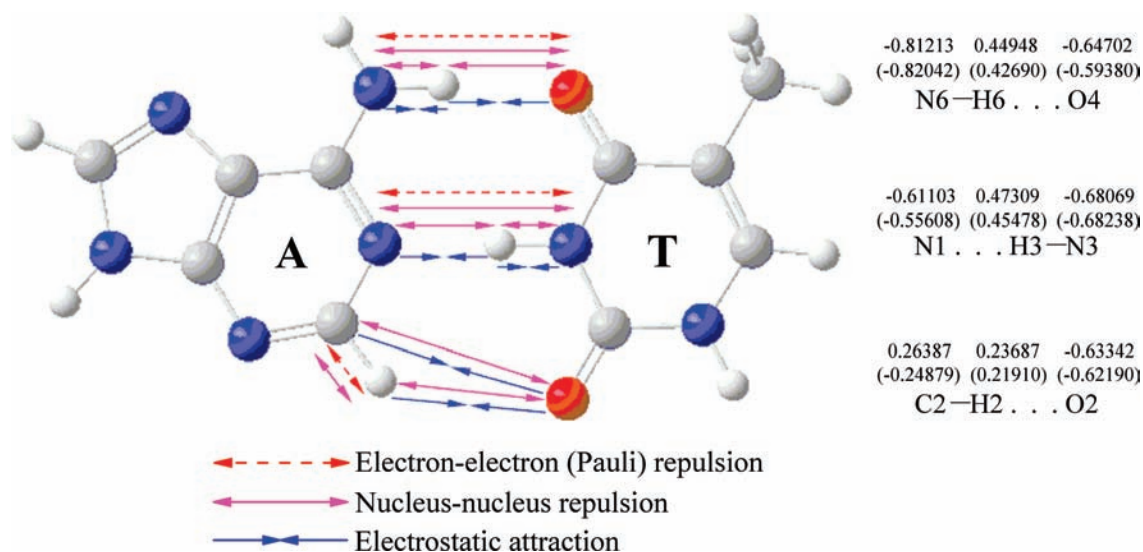


Figure 4. Electrostatic interactions along the three hydrogen bonds in the AT base pair. On the right are the natural atomic charges of the atoms involved in the hydrogen bonds (upper entry, in electrons) and the natural atomic charges of the corresponding atoms in the monomers A and T bases, which are given in parentheses (lower entry, in electrons).

larger slope ranging from 5.0 to 3.5 Å, and the interaction energy strengthens rapidly. This is attributed to the increasing van der Waals interactions which make the complex more stable. When reaching to 3.5 Å of the N1...N3 distance, the N3–H3...N1 hydrogen bond begins to form. The $\rho(\text{N1}\cdots\text{H3})$ is 0.01080 au, and its Laplacian $\nabla^2\rho(\text{N1}\cdots\text{H3})$ equals to 0.02566 au. The N6–H6...O4 hydrogen bond begins to form at 3.4 Å of the N1...N3 distance. The topological parameter $\rho(\text{O4}\cdots\text{H6})$ is 0.00826 au, and $\nabla^2\rho(\text{O4}\cdots\text{H6})$ is 0.02544 au at this point. The N6–H6...O4 and N3–H3...N1 hydrogen bonds and the C2–H2...O2 van der Waals contact strengthen with the decreasing distance between A and T bases. It can be seen from sharply increasing slope of the potential energy curve, in which the interaction energy gets more and more negative. When A and T bases are sufficiently close to each other, the Pauli and nucleus–nucleus repulsions come into effect and become stronger. The balance of these interactions makes the interaction energy curve goes through a minimum (i.e., the equilibrium position) and then becomes less and less negative.

Figure 3b is the curve for the change of N6–H6 bond length as a function of the N6...O4 distance. It shows that the N6–H6 bond exhibits a continuous lengthening when N1 atom comes closer to N3 atom. At the large distance, the N6–H6 bond length varies a little. From 5.5 to 4.6 Å, the N6–H6 bond is slightly lengthening with the gradually increasing van der Waals interactions. Because of the appearance of intermolecular hyperconjugative interactions, from 4.6 to 3.4 Å, the N6–H6 bond length increases rapidly. Ranging from 3.4 Å to the equilibrium position, the N6–H6 bond length sharply increases due to the strengthening of the hydrogen-bonding interactions. The equilibrium position is located at the place where the N6–H6 bond is lengthened, so the N6–H6...O4 hydrogen bond is red-shifted. In addition, we note that at the equilibrium position for AT base pair formation, when N6–H6...O4 hydrogen bond is considered, the negative charge on N6 decreases while the positive charge on H6 increases relative to those of A base, and the negative charge on O4 increases compared to that of T base (see Figure 4). It suggests that during the approach of the proton donor and acceptor, the $\text{H6}^{\delta+}\cdots\text{O4}^{\delta-}$ electrostatic attraction becomes larger, while the electrostatic attraction $\text{H6}^{\delta+}\cdots\text{N6}^{\delta-}$ may become smaller, and the electron–electron (Pauli) repulsion $\text{N6}^{\delta-}\cdots\text{O4}^{\delta-}$ may become smaller,

too. Although there exist nuclei repulsions, they are very weak. The final result is that the much stronger $\text{H6}^{\delta+}\cdots\text{O4}^{\delta-}$ electrostatic attraction predominates over other forces and elongates the N6–H6 bond, and its stretching vibrational frequency shifts to a lower value. Thus, it can be concluded that the N6–H6 bond elongation and its red shift are primarily caused by electrostatic interactions, as well as hyperconjugative interactions.

The curve for the change of N3–H3 bond length as a function of the N3...N1 distance (Figure 3c) are very similar in shape to that of Figure 3b. The equilibrium position is located at the place where the N3–H3 bond is lengthened, so N3–H3...N1 hydrogen bond is also red-shifted. Because in the N3–H3...N1 hydrogen bond, the negative charge on N3 decreases relative to that of the T base, while the positive charge on H3 increases, and the negative charge on N1 increases compared to that of A base (see Figure 4), they may make the $\text{H3}^{\delta+}\cdots\text{N1}^{\delta-}$ electrostatic attraction become larger, while the electrostatic attraction $\text{H3}^{\delta+}\cdots\text{N3}^{\delta-}$ and the electron–electron (Pauli) repulsion $\text{N1}^{\delta-}\cdots\text{N3}^{\delta-}$ become smaller. The nuclei repulsions are very weak. Consequently, the stronger $\text{H3}^{\delta+}\cdots\text{N1}^{\delta-}$ electrostatic attraction elongates the N3–H3 bond and lowers its stretching vibrational frequency. Thereby, besides hyperconjugative interactions, electrostatic interactions are also an important reason for the red-shifted N3–H3...N1 hydrogen bond.

As the above-mentioned predication, the shortening effects of repolarization and rehybridization do not play dominant roles in the origins of the red-shifted N6–H6...O4 and N3–H3...N1 hydrogen bonds. For the red-shifted N6–H6...O4 hydrogen bond, the increasing s-character of the N6 hybrid orbital in the N6–H6 bond and, the strengthening polarization of the N6–H6 σ bonding orbital as well as the weakening polarization of its σ^* antibonding orbital which lead to the increasing N6–H6 bond polarization are supposed to shorten the N6–H6 bond, but contrarily, the N6–H6 bond lengthens with their variations upon the approaching of A and T bases (see Figure 5a–c). Likewise, similar situations are observed for the red-shifted N3–H3...N1 hydrogen bond. As can be seen from Figure 6a–c, the N3–H3 bond lengthens with the increasing s-character of N3 hybrid orbital in the N3–H3 bond, with the strengthening polarization of N3–H3 σ bonding orbital and the weakening polarization of its σ^* antibonding orbital.

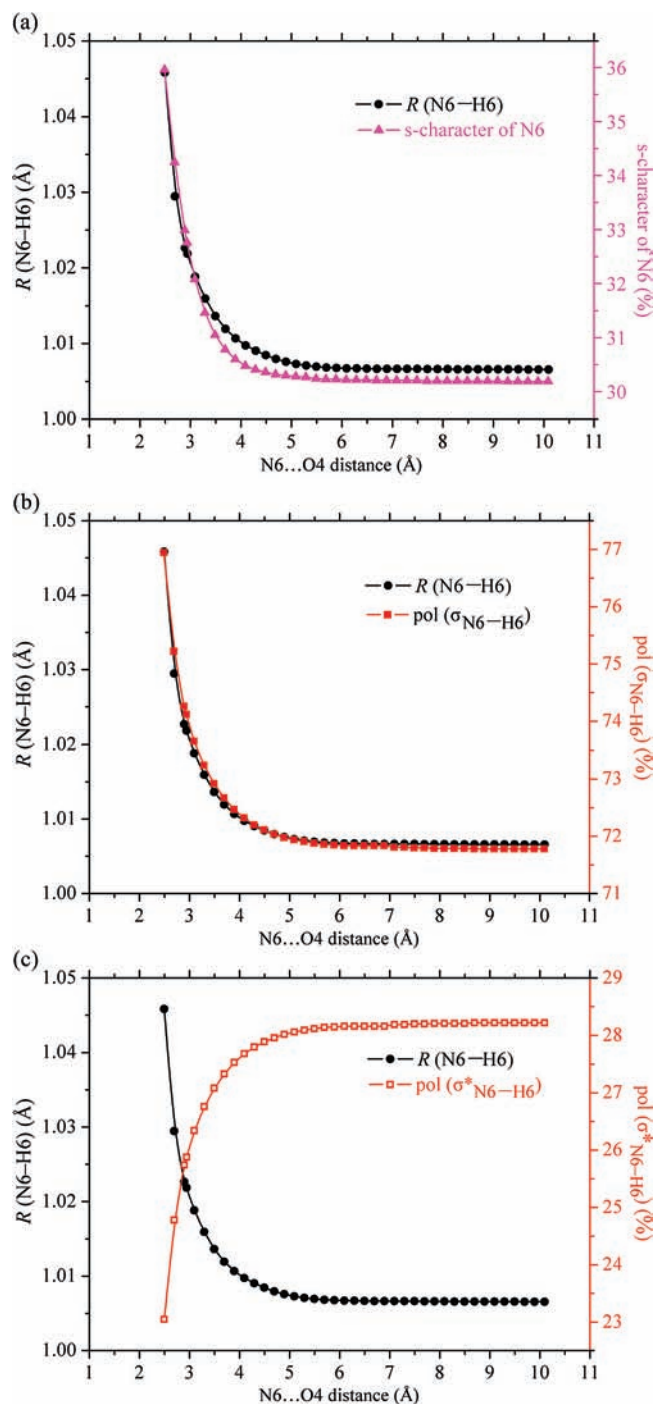


Figure 5. Correlations of the N6-H6 bond length with (a) s-character of N6-hybrid orbital in N6-H6 bond, (b) polarization of the N6-H6 σ bonding orbital, and (c) polarization of the N6-H6 σ^* antibonding orbital.

However, with respect to the C2-H2...O2 van der Waals contact, the curve of the C2-H2 bond length variation as a function of the C2...O2 distance is quite different (see Figure 3d). There are a few changes for the C2-H2 bond length at the large distance between the A and T bases. Ranging from 6.3 to 4.7 Å of the C2...O2 distance, the curve first appears as a small slope and then the slope gradually increases, which shows the processes of the C2-H2 bond contraction. It should be noted that 6.3 Å of the C2...O2 distance corresponds to 5.5 Å of the N1...N3 distance, at which the bond critical point of O4...H6 starts to appear. The increasing N6-H6...O4 and N3-H3...N1 van der Waals interactions from 6.3 to 4.7 Å

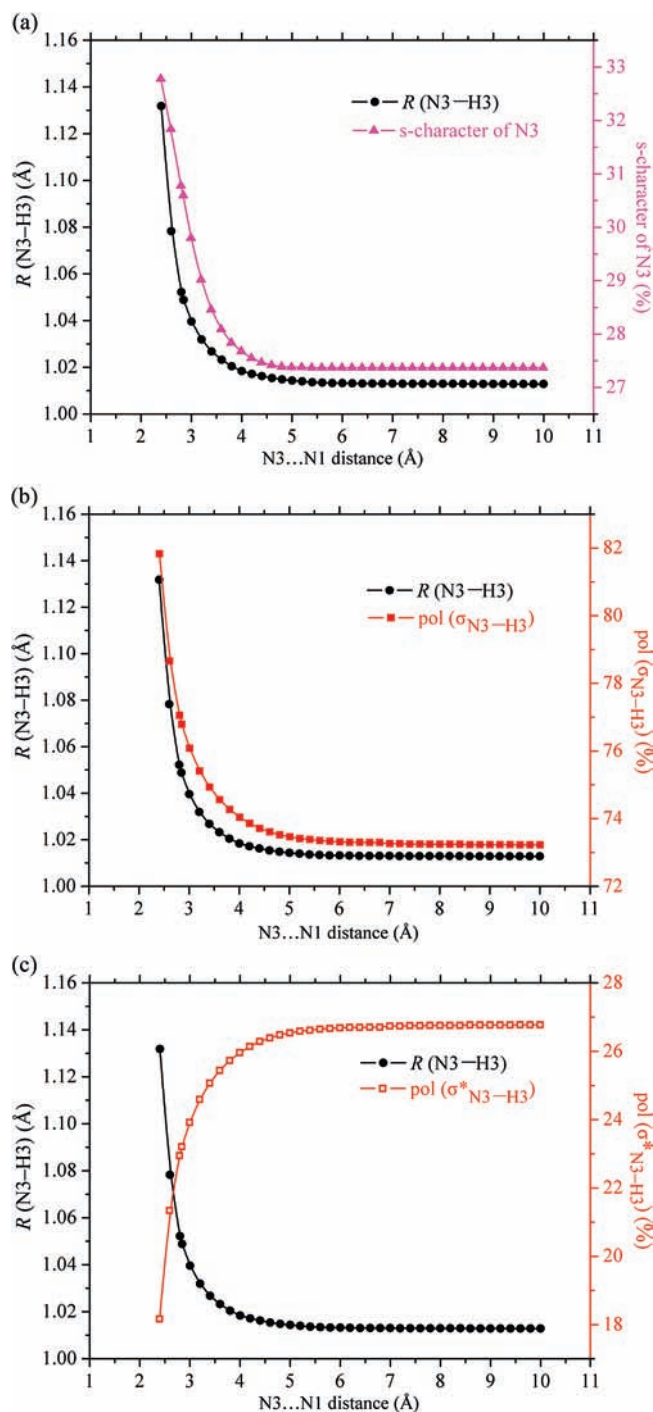


Figure 6. Correlations of the N3-H3 bond length with (a) s-character at N3-hybrid orbital of N3-H3 bond, (b) polarization of the N3-H3 σ bonding orbital, and (c) polarization of the N3-H3 σ^* antibonding orbital.

lead to the approach of A and T bases, and the two interactions have cooperative effects on the C2-H2 bond length change. In this process, the C2-H2 bond length gradually shortens with the increase of s-character of the C2 hybrid orbital in the C2-H2 bond, and of the C2-H2 bond polarization, which is due to its strengthening σ bonding orbital polarization and its weakening σ^* antibonding orbital polarization (see Figure 7a-c). It suggests that rehybridization and repolarization are important reasons for the C2-H2 bond contraction. Moreover, during the decreasing of the C2...O2 distance (from 6.3 to 4.7 Å), it can be seen from Figure 8 that the negative charge on O2 decreases, while both the positive charges on C2 and H2 increases. As a result,

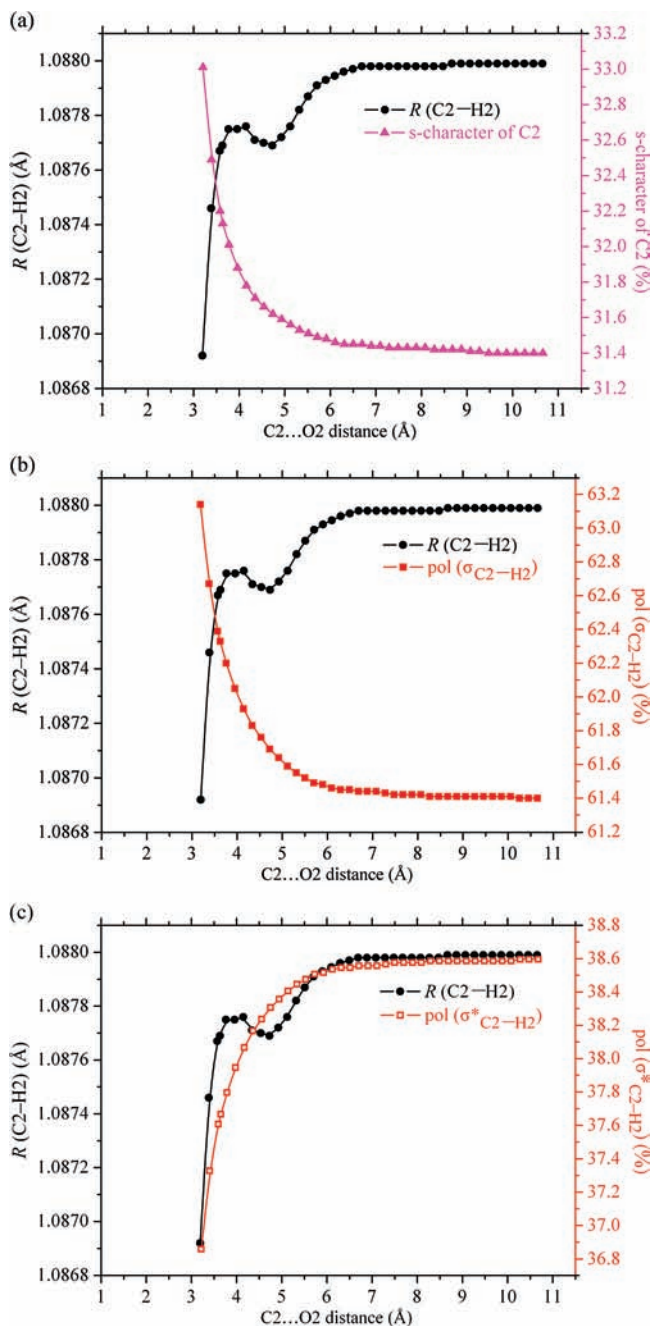


Figure 7. Correlations of C2–H2 bond length with (a) s-character at C2-hybrid orbital of C2–H2 bond, (b) polarization of the C2–H2 σ bonding orbital, and (c) polarization of the C2–H2 σ^* antibonding orbital.

the $\text{C2}^{\delta+} \cdots \text{H2}^{\delta+}$ electron–electron repulsion would grow stronger, while the $\text{H2}^{\delta+} \cdots \text{O2}^{\delta-}$ electrostatic attraction may become weaker. And during this process, the approach between the proton acceptor (O2) and the proton donor (C2–H2 bond) makes the $\text{H2} \cdots \text{O2}$ nucleus–nucleus repulsion grow stronger. Also, there exist $\text{C2}^{\delta+} \cdots \text{O2}^{\delta-}$ electrostatic attraction and $\text{C2} \cdots \text{O2}$ nucleus–nucleus repulsion, and $\text{C2} \cdots \text{H2}$ nucleus–nucleus repulsion, but they are very weak. The stronger $\text{H2} \cdots \text{O2}$ nucleus–nucleus repulsion may compress the C2–H2 bond. Surprisingly, after going through a local minimum where it is about 4.7 Å of the C2...O2 distance in Figure 3d, the curve starts to exhibit a negative slope. It shows that the C2–H2 bond starts to lengthen compared to the C2–H2 bond length at 4.7 Å of the C2...O2 distance. The reason may be that at this distance (corresponding to 4.0 Å of the N1...N3 distance), the

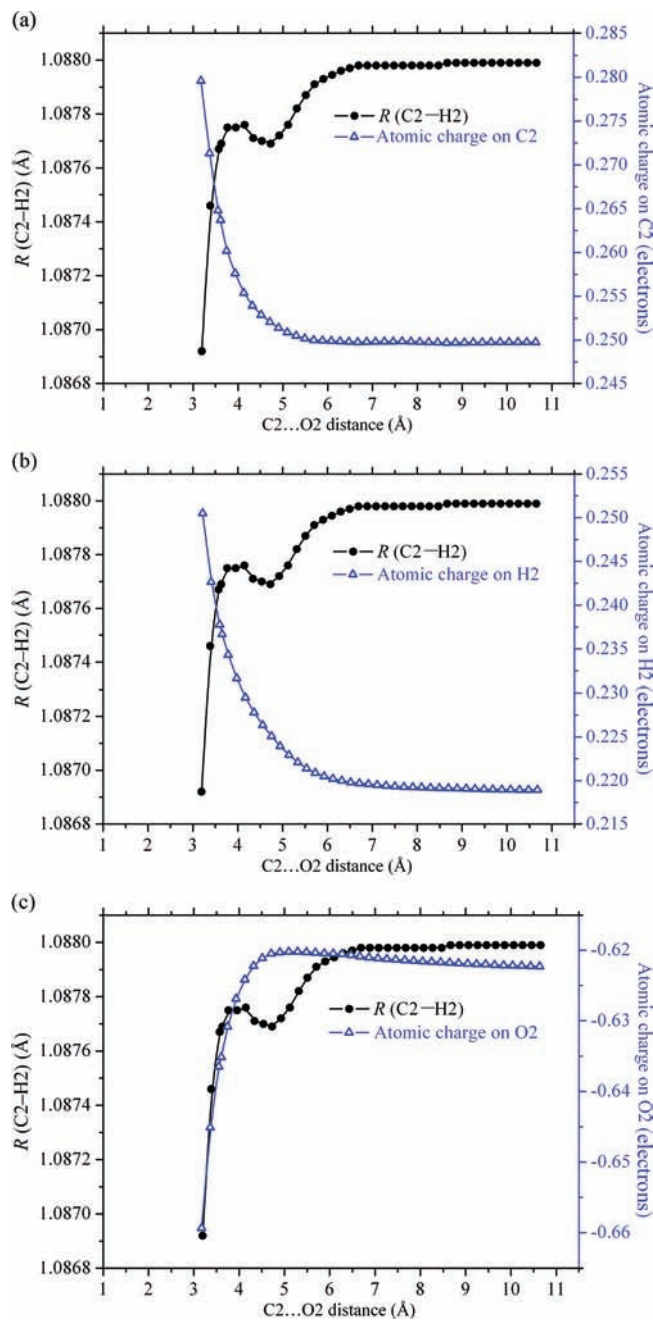


Figure 8. Correlations of C2–H2 bond length with (a) the natural atomic charges on C2 atom, (b) the natural atomic charges on H2 atom, and (c) the natural atomic charges on the O2 atom.

$\text{C2–H2} \cdots \text{O2}$ van der Waals interaction starts to form, the increasing negative charge on O2 (see Figure 8c) remarkably strengthens the $\text{H2}^{\delta+} \cdots \text{O2}^{\delta-}$ electrostatic attraction and elongates the C2–H2 bond. Moreover, the hyperconjugation that acts as a bond lengthening effect is also important. Nevertheless, the C2–H2 bond length then goes through a maximum and shortens again. It can be observed that from the maximum to the equilibrium position, the more positive charge on the C2 atom and the more negative charge on the O2 atom makes the $\text{C2}^{\delta+} \cdots \text{O2}^{\delta-}$ electrostatic attraction become stronger (see Figure 8a,c), thus resulting in the closer distance between H2 and O2, and the considerably increasing nucleus–nucleus repulsion between H2 and O2 forces the C2–H2 bond to contract. Additionally, the hybridization and polarization of the C2–H2 bond are also strengthening. These bond shortening effects balance with the bond lengthening effects, and then dominate

over them. Finally, the equilibrium position is located at about 3.63 Å of the C2...O2 distance where the C2–H2 bond is shortened, so the C2–H2...O2 van der Waals contact is blue-shifted. Therefore, it can be concluded that the reason for the complicated curve of the C2–H2 bond length changes as a function of the C2...O2 distance is that there is an intense competition between the bond shortening effects and the bond lengthening effects, they control the C2–H2 bond length changes, and the dominant one will determine the C2–H2 bond length variation and its frequency shift.

In regard to the physical reason for the blue-shifted hydrogen bond, another important viewpoint sees that the electric field effect induced by the electron donor Y leads to a shortening of the X–H bond.^{23,24,37–43} This theory has shed light on the origin of the contracted X–H bond and its blue shift. Therefore, we think that the blue-shifted C2–H2...O2 van der Waals contact in the AT base pair may also be explained by this theory. Analogous to the hydrogen-bonded complex, in the C2–H2...O2 contact, the proton donor C2–H2 is exposed to the electric field of the acceptor O2. Therefore, during the approach of A and T bases, the electric field induced by the acceptor O2 alters. It means that the electric field strength is changing. In general, the electric field strength is increasing with the decreasing donor–acceptor distance. As a consequence, the C2–H2 bond length varies with the electric field strength. It is similar to the electric field model considered by Hermansson and co-workers,^{23,24} Qian and Krimm,^{37–39} and Dannenberg and co-workers,⁴² which is used to investigate the nature of the blue-shifted hydrogen bond, especially for the hydrogen bond involving the C–H bond. In their studies, they observed that in some cases, the C–H bond shortens at small electric fields but lengthens at high electric fields.^{23,37,42} Similar phenomena are also observed for the C2–H2 bond from 6.3 Å to the maximum (see Figures 3d, 7, and 8). It can be explained by using the theories proposed by Hermansson,²³ Qian and Krimm,³⁷ and Dannenberg and co-workers.⁴² From 6.3 to 4.7 Å, the C2–H2 bond shortening is due to the interaction between the electric field created by the O2 atom and the negative dipole derivative of the C2–H2 bond,^{23,37} while from the 4.7 Å to the maximum, the C2–H2 bond lengthening compared to the C2–H2 bond length at 4.7 Å of the C2...O2 distance may be attributed to the decreasing electron density on the C2–H2 bond.^{23,42} But after going through a maximum, the C2–H2 bond starts to shorten again, this may be ascribed to the strengthening hybridization and polarization of the C2–H2 bond and short-range repulsive forces faced by the H2 atom. However, the factual situation should be more complicated in the C2–H2...O2 contact, and to interpret its blue shift, we must consider not only the electric field induced by the acceptor O2 but also exchange repulsive, dispersion, charge transfer, intramolecular intrinsic effects,^{23,38,39} and so on.

6. Conclusions

The controversy about whether there is a C–H...O hydrogen bond in the AT base pair^{11–13,17–20} has now been answered. The B3LYP/6-31G(d, p) level of theory is selected for the geometry optimization of the AT base pair and A and T bases, because it can provide the most accurate geometrical characteristics of the AT base pair. AIM and NBO analyses are performed at this level of theory. AIM analysis gives evidence to the existence of the C–H...O contact in the AT base pair as a van der Waals interaction rather than a hydrogen-bonding interaction. NBO analysis shows that there are two very weak intermolecular donor–acceptor orbital interactions corresponding to the C–H...O contact. The results indicate that the theory of method

and basis set adopted are very important to reflect the factual interactions between A and T bases in the AT base pair.

Hydrogen bonds N–H...O and N–H...N in the AT base pair are red-shifted, while the C–H...O van der Waals contact exhibits the opposite spectroscopic behavior as a blue shift. According to the AIM theory, the electron density ρ can be used to interpret the origins of their spectroscopic behaviors. The red-shifted N–H...O and N–H...N hydrogen bonds can be attributed to the decreases of electron densities in their N–H bonds upon AT base pair formation, while the blue shift of the C–H...O contact is due to the increase of electron density in its C–H bond. NBO analysis reveals that four chemical factors (intermolecular and intramolecular hyperconjugations, rehybridization, and repolarization) play different roles in their origins. We report a method by combining the electron density in the X–H (X = N, C) σ bonding orbital with that in the σ^* antibonding orbital to quantitatively estimate the effect of hyperconjugation. It is demonstrated that hyperconjugation acts as a bond lengthening effect for the X–H (X = N, C) bond in the AT base pair. Both rehybridization and repolarization result in the shortened X–H (X = N, C) bond in the AT base pair, but their effects on the red-shifted N–H...O and N–H...N hydrogen bonds are not dominant, whereas they play a crucial role in the blue shift of the C–H...O contact. While structural reorganization can act both as a bond lengthening effect and bond shortening effect, it may have different effects on the different X–H bond.

Apart from these factors, we have also considered the importance of the physical factors that include the attractive and repulsive interactions. At the equilibrium geometry of the complex, there is a competition between them. For the red-shifted N–H...O and N–H...N hydrogen bonds in the AT base pair, the stronger attractive interaction between the higher electronegativity Y (Y = O, N) and the positive H atom is the main reason for the elongation of the N–H bond and its red shift. With regard to the blue-shifted C–H...O van der Waals contact, the considerable nucleus–nucleus repulsion between H and O may be a factor leading to the C–H bond contraction and its blue shift. Another important factor may be the electric field induced by the acceptor O atom. Herein, we show that, for the first time, the theories for the blue-shifted hydrogen bond can also be successfully applied to explaining the blue-shifted van der Waals contact.

Acknowledgment. We thank Prof. Todd A. Keith for sending us a copy of the AIMAll (Version 08.11.06) program. This work was supported by the National Natural Science Foundation of China (No.20173023 and No.90203012) and Specialized Research Fund for the Doctoral Program of Higher Education of China (No.20020730006).

Supporting Information Available: Hyperconjugation interactions in the AT base pair and A and T bases. This material is available free of charge via the Internet at <http://pubs.acs.org>.

References and Notes

- (1) Jeffrey, G. A.; Saenger, W. *Hydrogen Bonding in Biology and Chemistry*; Springer-Verlag: Berlin, 1991.
- (2) Jeffrey, G. A. *An Introduction to Hydrogen Bonding*; Oxford University Press: New York, 1997.
- (3) Desiraju, G. R.; Steiner, T. *The Weak Hydrogen Bond*; Oxford University Press: Oxford U.K., 1999.
- (4) Scheiner, S. *Hydrogen Bonding*; Oxford University Press: New York, 1997.
- (5) Kryachko, E. S. *Hydrogen Bonding-New Insights*; Springer: Dordrecht, The Netherlands, 2006.

- (6) Buckingham, A. D.; Fowler, P. W.; Hutson, J. M. *Chem. Rev.* **1988**, *88*, 963.
- (7) Castleman, A. W., Jr.; Hobza, P. *Chem. Rev.* **1994**, *94*, 1721.
- (8) Muller-Dethlefs, K.; Hobza, P. *Chem. Rev.* **2000**, *100*, 143.
- (9) Watson, J. D.; Crick, F. H. C. *Nature* **1953**, *171*, 737.
- (10) Saenger, W. *Principles of Nucleic Acid Structure*; Springer: New York, 1984.
- (11) Leonard, G. A.; McAuley-Hecht, K.; Brown, T.; Hunter, W. N. *Acta Crystallogr., Sect. D* **1995**, *51*, 136.
- (12) Ghosh, A.; Bansal, M. *J. Mol. Biol.* **1999**, *294*, 1149.
- (13) Ghosh, A.; Bansal, M. *Acta Crystallogr., Sect. D* **1999**, *55*, 2005.
- (14) Grunenberg, J.; Goldberg, N. *J. Am. Chem. Soc.* **2000**, *122*, 6046.
- (15) Grunenberg, J.; Streubel, R.; Frantzius, G. v.; Marten, W. *J. Chem. Phys.* **2003**, *119*, 165.
- (16) Xie, Y.; Schaefer, H. F., III. *Z. Phys. Chem.* **2003**, *217*, 189.
- (17) Grunenberg, J. *J. Am. Chem. Soc.* **2004**, *126*, 16310.
- (18) Brandhorst, K.; Grunenberg, J. *ChemPhysChem* **2007**, *8*, 1151.
- (19) Shishkin, O. V.; Spomer, J.; Hobza, P. *J. Mol. Struct. (THEOCHEM)* **1999**, *477*, 15.
- (20) Guerra, C. F.; Bickelhaupt, F. M.; Snijders, J. G.; Baerends, E. J. *Chem.-Eur. J.* **1999**, *5*, 3581.
- (21) Asensio, A.; Kobko, N.; Dannenberg, J. J. *J. Phys. Chem. A* **2003**, *107*, 6441.
- (22) Quinn, J. R.; Zimmerman, S. C.; Bene, J. E. D.; Shavitt, I. *J. Am. Chem. Soc.* **2007**, *129*, 934.
- (23) Hermansson, K. *J. Phys. Chem. A* **2002**, *106*, 4695.
- (24) Pejov, L.; Hermansson, K. *J. Chem. Phys.* **2003**, *119*, 313.
- (25) Li, X.; Liu, L.; Schlegel, H. B. *J. Am. Chem. Soc.* **2002**, *124*, 9639.
- (26) Wang, J.-T.; Feng, Y.; Liu, L.; Li, X.-S.; Guo, Q.-X. *Chem. Lett.* **2003**, *32*, 746.
- (27) Fang, Y.; Fan, J.-M.; Liu, L.; Li, X.-S.; Guo, Q.-X. *Chem. Lett.* **2002**, *31*, 116.
- (28) Zierkiewicz, W.; Jurecka, P.; Hobza, P. *ChemPhysChem* **2005**, *6*, 609.
- (29) Gu, Y.; Kar, T.; Scheiner, S. *J. Am. Chem. Soc.* **1999**, *121*, 9411.
- (30) Gu, Y.; Kar, T.; Scheiner, S. *J. Mol. Struct. (THEOCHEM)* **2000**, *552*, 17.
- (31) Scheiner, S.; Gu, Y.; Kar, T. *J. Mol. Struct. (THEOCHEM)* **2000**, *500*, 441.
- (32) Scheiner, S.; Kar, T.; Gu, Y. *J. Biol. Chem.* **2001**, *276*, 9832.
- (33) Scheiner, S.; Grabowski, S. J.; Kar, T. *J. Phys. Chem. A* **2001**, *105*, 10607.
- (34) Joseph, J.; Jemmis, E. D. *J. Am. Chem. Soc.* **2007**, *129*, 4620.
- (35) McDowell, S. A. C. *Phys. Chem. Chem. Phys.* **2003**, *5*, 808.
- (36) McDowell, S. A. C. *J. Chem. Phys.* **2003**, *119*, 3711.
- (37) Qian, W.; Krimm, S. *J. Phys. Chem. A* **2002**, *106*, 6628.
- (38) Qian, W.; Krimm, S. *J. Phys. Chem. A* **2002**, *106*, 11663.
- (39) Qian, W.; Krimm, S. *J. Phys. Chem. A* **2005**, *109*, 5608.
- (40) Delanoye, S. N.; Herrebout, W. A.; van der Veken, B. J. *J. Am. Chem. Soc.* **2002**, *124*, 7490.
- (41) Hobza, P.; Havlas, Z. *Chem. Phys. Lett.* **1999**, *303*, 447.
- (42) Masunov, A.; Dannenberg, J. J.; Contreras, R. H. *J. Phys. Chem. A* **2001**, *105*, 4737.
- (43) Hermida-Ramon, J. M.; Grana, A. M. *J. Comput. Chem.* **2007**, *28*, 540.
- (44) Cubero, E.; Orozco, M.; Hobza, P.; Luque, F. J. *J. Phys. Chem. A* **1999**, *103*, 6394.
- (45) Hobza, P.; Havlas, Z. *Chem. Rev.* **2000**, *100*, 4253.
- (46) Hobza, P. *Phys. Chem. Chem. Phys.* **2001**, *3*, 2555.
- (47) Zierkiewicz, W.; Michalska, D.; Havlas, Z.; Hobza, P. *ChemPhysChem* **2002**, *3*, 511.
- (48) Alabugin, I. V.; Manoharan, M.; Peabody, S.; Weinhold, F. *J. Am. Chem. Soc.* **2003**, *125*, 5973.
- (49) Inagaki, S.; Takahiro, T. *Chem. Lett.* **2005**, *34*, 750.
- (50) Reed, A. E.; Curtiss, L. A.; Weinhold, F. *Chem. Rev.* **1988**, *88*, 899.
- (51) McDowell, S. A. C.; Buckingham, A. D. *J. Am. Chem. Soc.* **2005**, *127*, 15515.
- (52) Alabugin, I. V.; Manoharan, M.; Weinhold, F. A. *J. Phys. Chem. A* **2004**, *108*, 4720.
- (53) Alabugin, I. V.; Manoharan, M. *J. Comput. Chem.* **2007**, *28*, 373.
- (54) McDowell, S. A. C. *J. Chem. Phys.* **2003**, *118*, 4066.
- (55) McDowell, S. A. C. *J. Chem. Phys.* **2003**, *118*, 7283.
- (56) McDowell, S. A. C. *Chem. Phys. Lett.* **2003**, *368*, 649.
- (57) McDowell, S. A. C. *Chem. Phys. Lett.* **2003**, *377*, 143.
- (58) Hobza, P.; Spirko, V. *Phys. Chem. Phys.* **2003**, *5*, 1290.
- (59) Parreira, R. L. T.; Galembeck, S. E.; Hobza, P. *ChemPhysChem* **2007**, *8*, 87.
- (60) Chandra, A. K.; Parveen, S.; Zeegers-Huyskens, Th. *J. Phys. Chem. A* **2007**, *111*, 8884.
- (61) Solimannejad, M.; Scheiner, S. *J. Phys. Chem. A* **2008**, *112*, 4120.
- (62) Karpfen, A.; Kryachko, E. S. *Chem. Phys. Lett.* **2006**, *431*, 428.
- (63) Zhang, G.; Ji, A.; Chen, D. *J. Mol. Struct. (THEOCHEM)* **2008**, *853*, 89.
- (64) Zhanpeisov, N. U.; Ohta, K.; Bholey, J.; Hatanaka, K.; Fukumura, H. *Int. J. Quantum Chem.* **2005**, *105*, 376.
- (65) Chandra, A. K.; Parveen, S.; Das, S.; Zeegers-Huyskens, Th. *J. Comput. Chem.* **2008**, *29*, 1490.
- (66) Frisch, M. J.; Trucks, G. W.; Schlegel, H. B.; Scuseria, G. E.; Robb, M. A.; Cheeseman, J. R.; Zakrzewski, V. G.; Montgomery, J. A.; Stratmann, R. E.; Burant, J. C.; Dapprich, S.; Millam, J. M.; Daniels, A. D.; Kudin, K. N.; Strain, M. C.; Farkas, O.; Tomasi, J.; Barone, V.; Cossi, M.; Cammi, R.; Mennucci, B.; Pomelli, C.; Adamo, C.; Clifford, S.; Ochterski, J.; Petersson, G. A.; Ayala, P. Y.; Cui, Q.; Morokuma, K.; Malick, D. K.; Rabuck, A. D.; Raghavachari, K.; Foresman, J. B.; Cioslowski, J.; Ortiz, J. V.; Stefanov, B. B.; Liu, G.; Liashenko, A.; Piskorz, P.; Komaromi, I.; Gomperts, R.; Martin, R. L.; Fox, D. J.; Keith, T.; Al-Laham, M. A.; Peng, C. Y.; Nanayakkara, A.; Gonzalez, C.; Challacombe, M.; Gill, P. M. W.; Johnson, B. G.; Chen, W.; Wong, M. W.; Andres, J. L.; Head-Gordon, M.; Replogle, E. S.; Pople, J. A. *Gaussian 98*, revision A.09; Gaussian, Inc.: Pittsburgh, PA, 1998.
- (67) Lu, P.; Liu, G.-Q.; Li, J.-C. *J. Mol. Struct. (THEOCHEM)* **2005**, *723*, 95.
- (68) Simon, S.; Duran, M.; Dannenberg, J. J. *J. Chem. Phys.* **1996**, *105*, 11024.
- (69) Boys, S. F.; Bernardi, F. *Mol. Phys.* **1970**, *19*, 553.
- (70) Bader, R. F. W. *Atoms in Molecules: A Quantum Theory*; Oxford University Press: Oxford, U.K., 1990.
- (71) Bader, R. F. W. *Chem. Rev.* **1991**, *91*, 893.
- (72) Keith, T. A. AIMALL, Version 08.11.06; aim.tkgristmill.com, 2008.
- (73) Foster, J. P.; Weinhold, F. *J. Am. Chem. Soc.* **1980**, *102*, 7211.
- (74) Reed, A. E.; Weinhold, F. *J. Chem. Phys.* **1983**, *78*, 4066.
- (75) Reed, A. E.; Weinstock, R. B.; Weinhold, F. *J. Chem. Phys.* **1985**, *83*, 735.
- (76) Reed, A. E.; Weinhold, F. *J. Chem. Phys.* **1985**, *83*, 1736.
- (77) Carpenter, J. E.; Weinhold, F. *J. Mol. Struct. (THEOCHEM)* **1988**, *169*, 41.
- (78) Engel, T.; Reid, P. *Physical Chemistry*; Benjamin Cummings: San Francisco, 2005.
- (79) Brown, I. D.; Altermatt, D. *Acta Crystallogr., Sect. B* **1985**, *41*, 244.
- (80) Brown, I. D. *Acta Crystallogr., Sect. B* **1992**, *48*, 553.
- (81) Monajjemi, M.; Chahkandi, B.; Zare, K.; Amiri, A. *Biochemistry (Moscow)* **2005**, *70*, 366.
- (82) Spomer, J.; Leszczynski, J.; Hobza, P. *J. Phys. Chem.* **1996**, *100*, 1965.
- (83) Brameld, K.; Dasgupta, S.; Goddard, W. A., III. *J. Phys. Chem. B* **1997**, *101*, 4851.
- (84) Guerra, C. F.; Bickelhaupt, F. M. *Angew. Chem.* **1999**, *111*, 3120; *Angew. Chem., Int. Ed.* **1999**, *38*, 2942.
- (85) Guerra, C. F.; Bickelhaupt, F. M.; Snijders, J. G.; Baerends, E. J. *J. Am. Chem. Soc.* **2000**, *122*, 4117.
- (86) Bertran, J.; Oliva, A.; Rodriguez-Santiago, L.; Sodupe, M. *J. Am. Chem. Soc.* **1998**, *120*, 8159.
- (87) Mo, Y. *J. Mol. Model.* **2006**, *12*, 665.
- (88) Spomer, J.; Jurecka, P.; Hobza, P. *J. Am. Chem. Soc.* **2004**, *126*, 10142.
- (89) Seeman, N. C.; Rosenberg, J. M.; Suddath, F. L.; Kim, J. P.; Rich, A. *J. Mol. Biol.* **1976**, *104*, 109.
- (90) Neidle, S. *Principles of Nucleic Acid Structure*; Academic Press: London, 2007.
- (91) Novoa, J. J.; Sosa, C. *J. Phys. Chem.* **1995**, *99*, 15837.
- (92) Sule, P.; Nagy, A. *J. Phys. Chem.* **1996**, *104*, 8524.
- (93) Mo, O.; Yanez, M.; Elguero, J. *J. Chem. Phys.* **1997**, *107*, 3592.
- (94) Rablen, P. R.; Lockman, J. W.; Jorgensen, W. L. *J. Phys. Chem. A* **1998**, *102*, 3782.
- (95) Dkhissi, A.; Adamowicz, L.; Maes, G. *J. Phys. Chem. A* **2000**, *104*, 2112.
- (96) Dkhissi, A.; Adamowicz, L.; Maes, G. *Chem. Phys. Lett.* **2000**, *324*, 127.
- (97) Mariam, Y. H.; Musin, R. N. *J. Mol. Struct. (THEOCHEM)* **2001**, *549*, 123.
- (98) Rienstra-Kiracofe, J. C.; Tschumper, G. S.; Schaefer, H. F., III.; Nandi, S.; Ellison, G. B. *Chem. Rev.* **2002**, *102*, 231.
- (99) Datta, A.; Pati, S. K. *J. Phys. Chem. A* **2004**, *108*, 9527.
- (100) Dunning, T. H., Jr. *J. Chem. Phys.* **1989**, *90*, 1007.
- (101) Wiberg, K. B. *J. Comput. Chem.* **2004**, *25*, 1342.
- (102) Pauling, L. *The Nature of the Chemical Bond*, 3rd ed.; Cornell University Press: Ithaca, NY, 1960.
- (103) Taylor, R.; Kennard, O. *J. Am. Chem. Soc.* **1982**, *104*, 5063.
- (104) Steiner, T. *Angew. Chem.* **2002**, *114*, 50; *Angew. Chem., Int. Ed.* **2002**, *41*, 48.
- (105) Dabkowska, I.; Gonzalez, H. V.; Jurecka, P.; Hobza, P. *J. Phys. Chem. A* **2005**, *109*, 1131.

- (106) Yanson, I. K.; Teplitzky, A. B.; Sukhodub, L. F. *Biopolymers* **1979**, 18, 1149.
- (107) Pittner, J.; Hobza, P. *Chem. Phys. Lett.* **2004**, 390, 496.
- (108) Dabkowska, I.; Jurecka, P.; Hobza, P. *J. Chem. Phys.* **2005**, 122, 204322.
- (109) Jurecka, P.; Sponer, J.; Cerny, J.; Hobza, P. *Phys. Chem. Chem. Phys.* **2006**, 8, 1985.
- (110) Dedikova, P.; Pitonak, M.; Neogrady, P.; Cernusak, I.; Urban, M. *J. Phys. Chem. A* **2008**, 112, 7115.
- (111) Pitonak, M.; Riley, K. E.; Neogrady, P.; Hobza, P. *ChemPhysChem* **2008**, 9, 1636.
- (112) Pitonak, M.; Neogrady, P.; Cerny, J.; Grimme, S.; Hobza, P. *ChemPhysChem* **2009**, 10, 282.
- (113) Kock, U.; Popelier, P. L. A. *J. Phys. Chem.* **1995**, 99, 9747.
- (114) Popelier, P. L. A. *J. Phys. Chem. A* **1998**, 102, 1873.
- (115) Lipkowski, P.; Grabowski, S. J.; Robinson, T. L.; Leszczynski, J. *J. Phys. Chem. A* **2004**, 108, 10865.
- (116) Bone, R. G. A.; Bader, R. F. W. *J. Phys. Chem.* **1996**, 100, 10892.
- (117) Carroll, M. T.; Bader, R. F. W. *Mol. Phys.* **1988**, 65, 695.
- (118) Boyd, R. J.; Choi, S. C. *Chem. Phys. Lett.* **1986**, 129, 62.
- (119) Cioslowski, J.; Mixon, S. T. *Can. J. Chem.* **1992**, 70, 443.
- (120) Gibbs, G. V.; Cox, D. F.; Rosso, K. M. *J. Phys. Chem. A* **2004**, 108, 7643.
- (121) McKean, D. C. *Chem. Soc. Rev.* **1978**, 7, 399.
- (122) Hobza, P. *Int. J. Quantum Chem.* **2002**, 90, 1071.
- (123) Hobza, P.; Havlas, Z. *Theor. Chem. Acc.* **2002**, 108, 325.
- (124) Chocholousova, J.; Spirko, V.; Hobza, P. *Phys. Chem. Chem. Phys.* **2004**, 6, 37.
- (125) Yang, Y.; Zhang, W. J.; Pei, S. X.; Shao, J.; Huang, W.; Gao, X. M. *Sci China., Ser. B* **2007**, 50, 32.
- (126) Li, A. Y. *J. Phys. Chem. A* **2006**, 110, 10805.
- (127) Tang, K.; Shi, F. Q. *Int. J. Quantum Chem.* **2007**, 107, 665.
- (128) Liu, Y.; Liu, W.; Li, H.; Liu, J.; Yang, Y. *J. Phys. Chem. A* **2006**, 110, 11760.
- (129) Liu, Y.; Liu, W. Q.; Yang, Y.; Liu, J. G. *Int. J. Quantum Chem.* **2006**, 106, 2122.
- (130) Liu, Y.; Liu, W. Q.; Li, H. Y.; Yang, Y.; Cheng, S. *Int. J. Quantum Chem.* **2007**, 107, 396.
- (131) Nguyen, H. M. T.; Peeters, J.; Zeegers-Huyskens, Th. *J. Mol. Struct. (THEOCHEM)* **2006**, 792–793, 16.
- (132) Liu, Y. *Int. J. Quantum Chem.* **2008**, 108, 1123.
- (133) Zeegers-Huyskens, Th. *J. Mol. Struct. (THEOCHEM)* **2008**, 887, 2.
- (134) Kolandavel, P.; Nirmala, V. *J. Mol. Struct. (THEOCHEM)* **2004**, 694, 33.
- (135) Yang, Y.; Zhang, W. J.; Gao, X. M. *Int. J. Quantum Chem.* **2006**, 106, 1199.
- (136) Li, A. Y. *J. Chem. Phys.* **2007**, 126, 154102.
- (137) Pluhackova, K.; Hobza, P. *ChemPhysChem* **2007**, 8, 1352.
- (138) Li, A. Y. *Chem. Lett.* **2008**, 37, 596.
- (139) Wang, W.; Hobza, P. *Collect. Czech. Chem. Commun.* **2008**, 73, 862.
- (140) Flukiger, P.; Liithi, H. P.; Portmann, S.; Weber, J. Molekel, Version 4.3, Swiss Center for Scientific Computing: Manno, Switzerland, 2002; <http://www.cscs.ch/molkel/>.
- (141) Zhou, P.-P.; Qiu, W.-Y. *ChemPhysChem* **2009**, 10, 1847.
- (142) Yang, Y.; Zhang, W. *J. Mol. Struct. (THEOCHEM)* **2007**, 814, 113.
- (143) Bent, H. A. *Chem. Rev.* **1961**, 61, 275.

JP9035452